EXPERIMENTAL

VELOCITY PROFILES IN ANNULAR PASSAGES

VELOCITY PROFILES

IN

ANNULAR PASSAGES

By

THOMAS WESLEY RICKER, B.Eng.

A Thesis

Submitted to the Faculty of Graduate Studies

in Partial Fulfilment of the Requirements

for the Degree

Master of Engineering

McMaster University

October 1966

MASTER OF ENGINEERING (1966) McMASTER UNIVERSITY
(Mechanical Engineering) Hamilton, Ontario.

TITLE: Velocity Profiles in Annular Passages

AUTHOR: Thomas Wesley Ricker, B.Eng. (McMaster University)

SUPERVISOR: Doctor J. H. T. Wade

NUMBER OF PAGES: (vi) 53

SCOPE AND CONTENTS:

An experimental study of turbulent velocity profiles of water flowing in a vertical annular passage is reported in this thesis. Presented are profiles for eccentricities ranging from 0% to 80% and Reynolds numbers from 40,000 to 104,000 in an annulus having a 0.286 radius ratio.

Velocities were measured along five radii for all but the concentric configuration and the two arbitrarily chosen configurations are represented in the form of cross-sectional maps of the isovels. A method for deriving the powers N_1 and N_2 as defined by the equations

$$\frac{u}{u_m} = \left[\frac{(r_2-r)}{(r_2-r_m)}\right]^{N_2} \quad \text{and} \quad \frac{u}{u_m} = \left[\frac{(r-r_1)}{(r_m-r_1)}\right]^{N_1}$$

is suggested, and these powers were found for the two configurations investigated.

ACKNOWLEDGEMENTS

The author is grateful for the supervision and assistance provided by Doctor J. H. T. Wade during the planning and performing of this experimental study. He also extends his appreciation to Mr. R. Judd, Mr. N. Wilson and Dr. J. Medwell for their suggestions and guidance.

This investigation was financially supported by a National Research Council Grant No. A-1585.

TABLE OF CONTENTS

TEXT

1. Introduction
2. Literature Survey
3. Test Facility
   - 3.1 Test Rig
   - 3.2 Test Section
4. Experimental Procedure
5. Data Analysis
6. Discussion
   - 6.1 Accuracy of Results
   - 6.2 Friction Factor Results
   - 6.3 Reproducability and Check for Fully Developed Flow
   - 6.4 Velocity Profiles
7. Conclusions
8. Nomenclature
9. References
10. Illustrations

APPENDIX

1. Velocity Correlation
2. Velocity Profiles

LIST OF FIGURES

Figure 1 - Annulus Analysis, First Iteration (Taken from Deissler and Taylor (1))

Figure 2 - Schematic Arrangement of Test Facility Components

Figure 3 --Flow Path in the Test Section

Figure 4 - Exploded View of the Test Section

Figure 5 - Test Facility

Figure 6 - Obtuse Stagnation Probe

Figure 7 - Acute Stagnation Probe

Figure 8 - Double-tipped Stagnation Probe

Figure 9 - Traversing Mechanism and Measuring Block

Figure 10 - Error versus Velocity

Figure 11 - Velocity Field in a 36.5% Eccentric Annulus at a Reynolds Number of 80,000

Figure 12 - Revised Velocity Field in a 36.5% Eccentric Annulus at a Reynolds Number of 80,000

Figure 13 - Velocity Field in a 76.0% Eccentric Annulus at a Reynolds Number of 80,000

Figure 14 - Revised Velocity Field in a 76.0% Eccentric Annulus at a Reynolds Number of 80,000

Figure 15 - Theoretical Velocity Field in a 36.5% Eccentric Annulus at a Reynolds Number of 80,175

Figure 16 - Measured Velocity versus Theoretical Velocity along Three Measuring Radii

Figure 17 - Inner Wall Dimensionless Velocity Profile (36.5% Eccentricity, 80,000 Reynolds Number)

Figure 18 --Outer Wall Dimensionless Velocity Profile (36.5% Eccentricity, 80,000 Reynolds Number)

Figure 19 - Inner Wall Dimensionless Velocity Profile (76.0% Eccentricity, 80,000 Reynolds Number)

Figure 20 - Outer Wall Dimensionless Velocity Profile (76.0% Eccentricity, 80,000 Reynolds Number)

1. INTRODUCTION

The annular passage configuration has, for a number of years, been a topic of great interest both for its practical application, and from the academic point of view, as a method of testing theoretical and semi-empirical hypotheses.

The widest known practical application of the annular passage is the nuclear reactor rod with cooling water flowing axially around the outside of it. Because of the inter-relationship of fluid mechanics and heat transfer, a knowledge of the velocity fields in annular passage is the first step in predicting the heat transfer capabilities of a particular configuration.

Several methods of analytically finding velocity maps and profiles for eccentric annuli exist in the literature; however, very little experimental data, which could be used to assess the validity of these methods, exists.

The present paper presents experimental velocity profiles for an annulus with a 0.286 radius ratio using eccentricities from 0% to 80% and Reynolds Numbers from 40,000 to 104,000, with water as the working fluid.

2. LITERATURE SURVEY

A paper by Deissler and Taylor (1)* presents the first attempt to produce analytical velocity maps in concentric and eccentric annuli. Also shown in this paper is an analytical method of finding friction factors.

Briefly, the method of Deissler and Taylor begins by drawing the annulus and assuming a line of maximum velocities. Inherent in this assumption is also the assumption of the area segments and wall arc lengths used in calculating iteratively a more correct line of maximum velocities. This is illustrated in Figure 1. The following identity is developed using a force equilibrium equation:

$$\frac{\sqrt{\dfrac{\Delta A_2}{\Delta l_1 r_{l_1}}}}{\sqrt{\dfrac{\Delta A_1}{\Delta l_1 r_{2_1}}}} = \frac{F(y^+_{1m})}{F(y^+_{2m})} = \frac{u^+_{1m}}{u^+_{2m}}$$

To carry out an iteration, the areas and arc lengths which resulted from the assumption of a line of maximum velocities is found and is substituted into the left hand side of the identity. Also, by using the above areas and arc lengths, and assuming a Reynolds number, it is possible to calculate the parameters $F(y^+_{1m})$ and $F(y^+_{2m})$.** Using the logarithmic plot, u^+_{1m} and u^+_{2m} could then be found by using the calculated values for $F(y^+_{1m})$ and $F(y^+_{2m})$.

---

*Number in bracket refers to reference number.

**Parameters are defined in the Nomenclature.

Hence a value for the right hand side of the equation could be found and compared to the left hand side. New positions of the line of maximum velocities could then be assumed and the process repeated until the identity is satisfied.

To find lines of constant velocity(isovels) the following parameters were defined:

$$u_1^{++} = \frac{u_1}{\sqrt{\frac{-r_1 \, dp/dx}{e}}} \quad \text{and} \quad u_2^{++} = \frac{u_2}{\sqrt{\frac{-r_2 \, dp/dx}{e}}}$$

These were rewritten as:

$$u_1^{++} = \frac{u_1^{+} y_1^{+}}{r_1^{++} y_{1m} / r_1} \quad \text{and} \quad u_2^{++} = \frac{u_2^{+} y_2^{+}}{r_1^{++} y_{2m} / r_1}$$

All values in these definitions are known for elements for which the line of maximum velocity has been defined, except for the values of y_1/y_{1m} and y_2/y_{2m}.

It is then possible to calculate values of u_1^{++} and u_2^{++} as a function of parameters y_1/y_{1m} and y_2/y_{2m} along lines normal to the walls. Joining points of constant u_1^{++} and u_2^{++} yields the isovels.

Having defined lines of constant velocity, velocity gradient lines can be drawn. These new gradient lines can be used to approximate the new velocity lines for the adjacent areas.

Heyda (2) attempted to carry the work of Deissler and Taylor one step further by using a system of bipolar coordinates and by computerizing

the iterative process to produce velocity profiles. He used the assumption that the wall shear stress is constant. No sample solutions were produced by Heyda.

In an experimental thesis by Ivey (3), a correlation is given as follows for the location of the line of maximum velocities:

$$\left[\frac{r_2(r_m^2-r_1^2)}{r_m(r_m^2-r_2^2)}\right]^{1.25} = \left[\frac{(N_2+2)(N_2+1)}{(N_1+2)(N_1+1)}\right]^{1.75}$$

The values of N_1 and N_2 are the powers in the power law:

$$\frac{u}{u_m} = \left[\frac{(r_2-r)}{(r_2-r_m)}\right]^{N_2} \qquad \text{(outer wall)}$$

and

$$\frac{u}{u_m} = \left[\frac{(r-r_1)}{(r_m-r_1)}\right]^{N_1} \qquad \text{(inner wall)}$$

The paper presents powers for various Reynolds numbers in the range from 11,129 to 25,770 for annuli with radius ratios 0.202, 0.269, 0.307, 0.350, 0.422, 0.432, 0.495, 0.504, 0.507, 0.621 and 0.698. No correlation between powers and either equivalent diameters or diameter ratios was given. Also, no change in power as a function of Reynolds number in the range studied was found.

Wilson (4) further modified previous theoretical work, and with the aid of the computer predicted velocity fields for both concentric and eccentric annuli. Once more, a system of bipolar coordinates was employed. A Van Driest (5) velocity profile was used rather than the logarithmic plot used by Deissler and Taylor. A force balance on inner and outer

incremental areas was carried out, and hence inner and outer shear stresses as a function of location around the wall were found.

In an experimental paper, Lee and Barrow (6) present a velocity field plot along with work on heat transfer and friction factors. Their apparatus drew air through an annulus test section which was equipped with flanges at the measuring stations which could be rotated to probe the entire field. They checked for fully developed flow by finding the pressure drop for successive sections, and assumed that the flow was fully developed where the pressure drop remained constant over two successive sections.

3. TEST FACILITY

3.1 Test Rig

Experimentation was carried out with a closed loop circuit which continuously recirculated water through the test section. A schematic of the system is shown in Figure 2, and the flow through the test section is shown in Figure 3. This equipment was first reported in Reference (8).

The circulating pump used was a Worthington Model 6QAU gear pump operating at 1750 revolutions per minute. The output from this pump was a constant 55 U.S. gallons per minute. The flowrate through the test section could be regulated manually by operating a valve in a by-pass circuit which recirculated the excess flow through the pump.

The water flowrate was measured in a calibrated flow meter section employing an orifice plate designed in accordance with the British Standard Code for Flow Measurements (Bs 1042:1943). Pressure differential across the orifice was measured with a vertical mercury manometer. Upstream and downstream of the orifice plate, a straight section of pipe was used to insure that the flow conditions through the orifice were the same whether the section was in a loop or removed for calibration purposes. Pressure drop across the orifice varied from 1.6 inches to 9.0 inches of mercury. Differential pressures could be measured to $\pm$ 0.05 inches of mercury. The maximum possible error in the corresponding flowrate measurement was approximately 5%.

The cooler section, which was required in the circuit to keep the temperature of the water from escalating during long runs, was a Heliflow Model 9xF-165 heat exchanger. Mains water was used as the cooling fluid.

The flow of mains water through the exchanger could be regulated manually by means of a valve, and an indication of the flowrate of cooling water was given by the pressure differential across an orifice which was located in the cooling water conduit.

A 5.0 U.S. gallon capacity head tank was joined into the loop to accomodate expansion of the water. The head tank was mounted approximately four feet above the highest point in the circuit to ensure that water completely filled the system at all times.

3.2 Test Section

The test section consisted of an inner and an outer tube held vertically by a stainless steel housing at each end. The assembly is shown in Figures 4 and 5.

The inner tube had a 0.50 inch outside diameter. At a point 14.0 inches from each end were four threaded studs, each at 90° to the other. Onto these studs were fitted 1/8 inch diameter plastic legs which were machined to lengths corresponding to specific eccentricities. The tips of the legs touched the inside of the outer tube when assembled, and acted as a means of steadying and aligning the inner tube. Each end of the inner tube was held in place by a tapered teflon bushing. A threaded brass nut with an external thread and an internal taper screwed into the stainless steel housing. The bushing was clamped between the nut and the housing thus affecting a leakproof seal and at the same time gripping the inner tube firmly. The bushing was mounted eccentrically in the housing

The 48.0 inch long outer tube was acrylic plastic with a 1.75 inch outside diameter and a 1/8 inch wall thickness. Each end of the outer tube

was mounted in a hub which in turn fitted into the stainless steel housing and was held in place by a clamping nut. Sealing between the hub and the housing, and also between the tube and the hub, was affected by the use of "O" rings. When assembled on the test rig, the outer tube protruded into the housings and left only about 1/2 inch clearance between the end of the tube and the end of the housing. This created a flow pattern as shown in Figure 3. The configuration caused the water to be turned abruptly through 180° at the entrance, producing a high turbulence level, as witnessed by the large fluctuations in pressure which had to be damped out. This large turbulence level was desirable in producing a rapid developement of the velocity profile.

The hubs in which the tube was mounted were machined eccentrically so that the tube was not at any time concentric with the housing. However, by rotating the hubs, and by adjusting the lengths of the legs which were mounted on the inner tube, one could, with this particular diameter outer tube, produce eccentricities between 0% and 100%. This was possible because both inner and outer tubes were mounted eccentrically with respect to the housings.

Three points were provided along the length of the tube through which the stem of a dial gauge could be placed. These were provided to produce an accurate method of knowing the eccentricity at the three points as well as the one which was obtained using the pitot probe as a measuring device. Hence, the inner tube could be set up to less than 2% deviation in eccentricity per foot.

The outer tube could be rotated around its own axis during measuring and setting up a test.

The probe station consisted of a 2 inch by 2.5 inch by 2.5 inch block of acrylic plastic, machined concave on one side and glued to the tube so that the tip of the probe, when in place, was 36.0 inches from one end of the tube, and when reversed, 10.0 inches from the other end. The block was designed with two static pressure taps which were drilled when the block was in place. When checking for flow development, the tube could be placed such that the measuring station was in a downstream position, and then could be removed and be turned end for end so that the measuring station was in an upstream position. The distance between upstream and downstream stations was 24.0 inches. One static pressure tap could be used while in an upstream position, the other while in the downstream position.

As well as the two static pressure taps in the measuring block, there were two static pressure taps at 180° from the block taps. One further pair of taps were located 25.0 inches from the stem of the probe, these taps being at 180° to each other. The static pressure taps which were not an integral part of the block consisted of pieces of 1.0 inch diameter acrylic rod, 3/4 inch long, concave on one end. These were glued to the outer tube, drilled and tapped to receive an "O" ring type "Swage-lok" tube fitting.

All pressure tap holes were made 1/32 inch in diameter and were carefully drilled to ensure there were no burs on the inside surface, and also that the hole was perpendicular to the wall.

The pressure tap holes in the block were made by inserting a 1/8 inch copper plug with a 1/32 inch hole in the center of it. The end of the plug was machined to fit the inside surface of the outer tube.

It was hoped this metal plug would provide a suitable electric contact which could be used to locate the probe with respect to the wall. It was found that the conductivity of the water made this unfeasable. For this reason the probe was lengthened such that the tip of the probe protruded 1/8 inch upstream of the pressure tap. This pressure tap was used only for measuring a manifolded static pressure drop over a 24.0 inch length. For purposes of velocity measurements the static pressure tap at 180° from the position of the probe was used.

Figures 6,7, and 8 show the three types of stagnation probes used. The stems of the probes in all cases were made of 0.072 inch O.D. stainless hypodermic tubing. The double tipped probe was used where the space between outer and inner wall permitted. This eliminated the necessity of starting a traverse with one probe which would touch one wall, and then switching to another probe during the traverse in order that the other wall be touched.

The tips of the probes were duck-billed, having 0.003 by 0.028 inch openings at the tips. The duck-billed shape was used to reduce the error due to the displacement effect near the wall. The probe, however, was too large to probe the sub-layer.

The hole in the measuring block through which the probe was inserted was a stepped hole. The outer hole was threaded to take a 7/8 inch brass plug. The inner hole was 3/8 inch in diameter, 1/8 inch deep. A stepped split brass plug, machined to fit the inside wall of the tube and drilled to mate with a dowel pin, fitted around the probe, and could be inserted into or removed from the 3/8 inch hole by means of a threaded rod which could be screwed into the face of the bushings for handling purposes.

The 7/8 inch brass plug was tapped and spot faced to receive a 1/16 inch "O" ring type "Swagelok" fitting. This fitting had to be drilled out to take the stem of the stagnation probe. The plug and fitting had to be mounted onto the stem during the assembly of the stagnation probe.

Sealing between the 7/8 brass plug and the measuring block was done using an "O" ring. Another "O" ring was used between the 7/8 inch plug and the split bushing in order to keep the bushings in place.

Figure 9 shows the probe station and traversing mechanism used. The traversing mechanism was supported by a 1/2 inch keyed rod which was clamped to the outer pipe. The micrometer head was held stationary and the tip of the micrometer screw butted against the slide. The slide was grooved and threaded to allow the stem of the stagnation probe to be clamped to it. Clamping surfaces were made of fibre to prevent crushing of the probe.

The reproducability of positioning was found to be about $\pm$ .002 inch. This reproducability error was due to the fact that the wall had to be located with the probe visually, and, as the optic qualities of the plastic outer tube were not good, some amount of positioning error was inevitable.

All test section pressure measurements were taken using a differential transducer.* The transducer was a variable reluctance type, and had a 0 to 5 volt nominal output for a 0 to 2 psi pressure differential. The transducer was calibrated using a micromanometer** from 0 to 10 inches

*Pace, Model CPSI.

**Meriam, Model 34FB2, 10 inches of water maximum.

of water and a water-filled "U" tube manometer above 10 inches. Hence, two ranges of error occurred: $\pm$ .005 inch of water in the range of 0 to 10 inches differential, and $\pm$ .05 inch of water above 10 inches of water differential pressure.

The voltage readings were taken using a digital voltmeter.* The error involved with this instrument was $\pm$ .005 volts.

*Franklin Electronics, Model 550.

4. EXPERIMENTAL PROCEDURE

The water in the system was unfiltered mains water which was changed periodically to ensure contamination-free flow. A coarse fibre-glass screen filter was used in the system to keep the plastic legs from going through the pump during testing, should one break off. Air bleeds were provided at two suitable points in the system.

During the initial set-up, water from the mains was continuously run into and out of the system, carrying with it any air bubbles which might have been trapped in the system.

When assembled with a set of acrylic legs corresponding to the eccentricity which was to be studied, the eccentric hubs which held the outer tube could be rotated and the tube brought to bear against the legs in such a manner as to maintain the most accurate setting of the eccentricity. The actual eccentricity was found by inserting the stem of a dial gauge through one of the three stations along the tube designed for this purpose and by rotating the outer tube. Also, with the dial gauge in place one could locate the line of maximum separation to within $\pm 2\frac{1}{2}^{\circ}$. Having thus located the line of maximum separation, a protractor could be clamped to the test section such that the zero on the protractor corresponded to a scribe mark on the outer tube.

Testing commenced by bringing the water temperature within a specified range ($100^{\circ}F \pm 10^{\circ}$). The outer wall was located visually with the tip of the stagnation probe and velocity head readings were then taken across the traverse at convenient intervals until the inner wall was reached. The probe was then relocated at the outer wall, the outer tube was rotated to a new radius and a new traverse was made. Five radial

traverses were made for each eccentric configuration investigated. Two radial traverses were made for the concentric cases investigated in order that a check for a symmetrical flow pattern be made.

For measurement of the static pressure drop along the tube, the upstream static pressure taps were manifolded together into the high pressure side of the transducer, and the downstream taps were manifolded into the low pressure side. Manifolding and selection of pressure differentials to be measured were effected using a system of valves.

It was found that, due to the extremely high sensitivity and fast response time of the transducer, the pressure fluctuations due to turbulence were recorded by the transducer. Since the digital voltmeter was virtually without inertia, it was impossible to obtain an average reading without damping. Hence a 5,000 μf capacitor was used across the terminals to reduce the fluctuations, in most cases, to $\pm$ .005 volts. In some cases it was necessary to use 10,000 μf to achieve the desired amount of damping.

Approximately 5 minutes were required for the capacitor to charge before an accurate reading could be taken.

In order to check for fully developed flow, the outer tube was turned end for end, and the stagnation probe was turned to face upstream.

The following readings were taken:

1) probe position
2) probe tip (outer or inner tip)
3) pressure differential between stagnation probe and static tap
4) pressure drop across a 24.0 inch section.

5. DATA ANALYSIS

Because of the quantity of data obtained, a graphical presentation was used. In the appendix, Figure i indicates the five lines along which readings were taken, 180° corresponding to the line of minimum separation, and 0° corresponding to the line of maximum separation.

Figure ii indicates the profiles obtained for the nominal 0% eccentricity. The measured eccentricity was 3%, but according to Ivey (3), little change occurs between a 0% eccentric and a 3% eccentric profile.

Figures iii through xvi show velocity profiles along five radii for a particular Reynolds number and eccentricity. While plotting these results, seven points (approximately 0.9% of the results) had large deviations from smooth curves. These were probably the result of not letting the damping condenser charge fully before taking the readings, and hence were eliminated from the graphical representation.

Results of the experimental differential pressures were found as voltages. From a calibration plot, the head in inches of water was found. From a second plot of the velocity versus head, the velocity was found in feet per second. This method was used since the volume of data was most efficiently analyzed in this way. Maximum errors involved in correlating using calibration curves and velocity versus stagnation head curves were 0.05 inches of water and 0.01 ft./sec. respectively.

The resulting maximum error, since low and high range calibration and velocity versus head curves were used, was about 1%.

Having plotted the velocities as a function of radius as shown in Figures ii to xvi in the appendix, the velocity fields could then be

drawn by selecting a particular velocity, finding in the profile plot how far this velocity occurs from the wall, and plotting it on the cross-sectional configuration as shown in Figure i.

The results of this type of plot are shown in Figures 11 to 14 for an eccentricity of 40% and 80%. Figures 11 and 13 show the information taken directly from the profiles. Figures 12 and 14 show the information revised, smoothing curves, making them orthoginal at the line of maximum separation, and showing possible shape of the curves where no data is available.

In Figures 17 through 20 the dimensionless profiles are plotted as a function of dimensionless distances from the wall. The velocity was non-dimensionalized by dividing it by the maximum velocity along the particular radius being analyzed.

The dimensionless distance for the outer wall was,

$$r_2^+ = \frac{r_2 - r}{r_2 - r_m}$$

and for the inner:

$$r_1^+ = \frac{r - r_1}{r_m - r_1} .$$

To obtain the inner profile, it was felt that the profile should be plotted along lines perpendicular to the inner wall. Hence, the dotted lines shown in Figures 11 and 13 were drawn radially from the surface of the inner tube to the point of intersection of the line of maximum velocity and the measurement radii. Velocity profiles along these lines could then be obtained using the reverse of the procedure used to draw the velocity

fields, and hence data could be obtained for drawing the dimensionless plot for the inner wall.

6. DISCUSSION

6.1 Accuracy of Results

This section endevours to indicate the maximum magnitude of the errors in the experiment. The maximum accumulative error is also presented. It should be noted that this value is higher than would actually occur, since it is very improbable that the maximum errors would occur all at once.

Since it is the concern of this thesis to present velocity profiles, then the most important error to consider is the one in the velocity. This error was due to two things. First, the correlation error which resulted from using calibration curves produced a maximum error of $\pm$ 1%. The second and more important error is due to "zero shift". Because of hysterisis of the diaphram in the transducer, the ability to reproduce a zero setting of the transducer was quoted as $\pm$ 1% of the full scale or $\pm$ 0.05 volts. When high velocities were being recorded, this represented only a small error. However, due to the shape of the velocity versus head curve, and the fact that the relative error increases as the head differential decreases, the error at low velocities was found to be very significant. Figure10 shows the addition of the two errors.

The error in reproducing the position of the probe, as previously stated, was $\pm$ 0.002 inch.

One further error inherent in positioning of the probe occurred when the probe approached the wall at an oblique angle. If the probe was not pointed directly upstream, the position error recorded could be very large for a relatively small deviation in the angle of the probe. (This

error was in fact found to occur in the 40% eccentricity which was transformed into a velocity field plot). To compensate for this error, in the process of drawing the velocity field, the profiles were started at both inner and outer wall, and any overlap or discrepancy was smoothed out at the line of maximum velocities. Due to large uncertainties in the position of the line of maximum velocities, it was felt that by allowing the descrepancy to occur in this area, it produced the best possible result.

Further errors occurring are listed below:

Error in outer tube diameter	$\pm$ .015 inch
Error in inner tube diameter	$\pm$ .0025 inch
Error in distance between static pressure taps	$\pm$ .125 inch
Error in volumetric flowrate:	
Instrument error	$\pm$ 5%
Flowrate fluctuations	$\pm$ 1%
Outer and inner diameters	$\pm$ 1.5%
Kinematic viscosity	$\pm$ 6%
Error in Reynolds number	$\pm$ 13.5%

6.2 Friction Factor Results

A random sample of friction factors were taken as a means of checking the accuracy of the static pressure holes. It was found that the friction factors were about 2% higher than those given in the literature, indicating that the construction of the static pressure holes was acceptable. The fact that the friction factors were slightly higher than those found in the literature indicates that the profile was developing over the section measured.

6.3 Reproducibility and Check for Fully Developed Flow

After deciding to use a double tipped probe, the question of probe interaction arose. In order to check for interaction, a traverse was made of the concentric case with the double tipped probe in the downstream position. At a later date a second traverse was made, this time using the acute and obtuse probes to make the traverse. It was found that about 2% deviation occurred, the double tipped probe giving higher readings than the single tipped probes. It was felt that this deviation was due, possibly, to a slight difference in the flow rates. However, it was concluded from this, that both reproducability of readings and results with the double tipped probe were of such quality that testing could proceed.

In checking for fully developed flow, it was found that a large change in profile shape occurred over the 24.0 inches between measuring positions, indicating a rapid development in profile. It was also found when doing tests on the concentric case that symmetric flow did not occur at the upstream measuring position, but did occur at the downstream one. Again this indicates a very rapid development induced by the turbulence due to entrance conditions.

Since the difference between the two profiles only indicates that a development has occurred, and not how much development has taken place, it was felt that a comparison with existing data was in order. In Figure ii the dotted line indicates a developed profile found by Goel (7) for a radius ratio.of 0.3 and a Reynolds number of 30,500 in air. It can be seen that the maximum difference in this profile and the profile having the 40,000 Reynolds number is only 3%. This discrepancy could

occur because of differences in physical size and radius ratio. The effect of Reynolds number can be seen in that the position of the maximum velocity in Goel's work (having a Reynolds number of 30,500) is displaced towards the outer wall with respect to the position of maximum velocity in the present work (having a Reynolds number of 40,000).

6.4 Velocity Profiles

Velocity fields were drawn for a 40% and an 80% nominal eccentricity configuration with a Reynolds number of 80,000. These were drawn in a manner shown in Figure i of the Appendix. From these two fields the dimensionless profiles for both inner and outer walls were found. The results of the plotting of these profiles are seen in Figures 17 through 20. Indicies of the power law were found by overlaying the velocity profiles with power law curves, and by choosing the best agreement. When plotting the velocity profiles as a log plot, it was found that, due to the fact that the lines did not coincide, and that there were only a few points per line, the method of overlaying was more accurate in finding the indicies.

For the 40% eccentricity and 80,000 Reynolds number, the power for the inner wall was found to be 1/11, and 1/9 for the outer wall. In the 80% eccentricity and 80,000 Reynolds number situation, the power for the inner wall was found to be 1/14, while the outer wall power was 1/13. This is in agreement with existing literature inasmuch as the power for the inner wall is smaller than that of the outer wall. It has been shown

that this is an effect of the lateral curvature of the inner wall(9).

The purpose in analyzing an 80,000 Reynolds number situation was two-fold. First, the error versus velocity curve shown in Figure 10 indicates that the high velocities can be measured more accurately than low velocities with the present apparatus. Second, it was felt that secondary flow in the high Reynolds number flow would be small; therefore, a comparison could be made with the theoretical work of Wilson (4) since this theoretical work does not consider the effects of cross-flow. An arbitrary choice was made between the 104,000 and 80,000 Reynolds number flows.

Plotted in Figure 15 is a theoretical velocity field by Wilson for a 36.5% eccentricity and an approximate Reynolds number of 80,000. A difference in the theoretical curves and the experimental curves is shown in Figures 11 and 12. The amount of deviation, however, is difficult to judge since the experimental curves are not complete, due to a lack of data over the entire cross-section.

It may be noted, however, that the deviation is consistent. Figure 16 shows the actual velocities plotted against the theoretical velocities. It can be seen that along the 45° line, the theoretical velocities are higher than the actual ones, while along the 90° line they are about the same, and along the 135° line, the theoretical velocities are lower than the actual ones. This would tend to indicate that cross-flow does have a large bearing on the velocity fields even at a 40% eccentricity.

7. CONCLUSIONS

An experimental study of velocity profiles in annular passages using seventeen sets of parameters has been carried out, and the results presented in graphical form. Velocity field diagrams have been presented for two arbitrary configurations. These have been compared to a theoretical correlation by Wilson (4). A consistent deviation between theoretical and experimental results has been shown, indicating that secondary flow may play a very large role in the velocity fields.

A method of correlating velocity profiles at inner and outer walls has been presented, and four representative values for the power in the power law have been given. The power for the 40% eccentric configuration and a Reynolds number of 80,000 for the inner wall was 1/11 and for the outer wall 1/9. The powers for the 80% eccentric configuration and a Reynolds number of 80,000 were found to be 1/14 for the inner wall, and 1/13 for the outer wall. This agreed with the literature inasmuch as the effect of lateral curvature produces a lower power on the inner wall than on the outer.

The present work indicates that future study should include a much more detailed study of the cross-section, using many more measuring radii along which to find velocity than are used here. Some method of probing perpendicular to the inner wall as well as to the outer wall would be an improvement on the present apparatus.

The test section length should be increased to dispell any doubts as to whether or not flow is fully developed. Furthermore, the physical

size of the annulus should be increased in order that the probe interference with the flow is minimized and the relative error in the position of the probe is kept to a minimum. The use of air as a working fluid would solve the technical problem of leaks in the system.

8. NOMENCLATURE

Arabic Symbols	Description	Units
ΔA	Incremental area	ft^2
Δl	Incremental length	ft
N	Power as defined by the power law (see page ii)	
p	Pressure	lb/ft^2
r	Radius	ft
r^+	Dimensionless distance (see page 16)	-
r_1^{++}	Inner tube radius parameter: $r_1^{++} = \sqrt{\frac{-r_1 \, dp/dx}{\rho}} \Big/ \frac{\mu}{\rho}$	-
u	Local velocity	ft/sec.
u_m^+	Velocity parameter: $u_m^+ = \frac{u}{\sqrt{\tau_o/\rho_o}}$	-
u^{++}	Velocity parameter: $u^{++} = \frac{u}{\sqrt{\frac{-r_1 \, dp/dx}{\rho}}}$	ft^{-1}
x	Axial distance	ft
y_{1m}	Distance from inner wall to line of maximum velocity	ft
y_{2m}	Distance from outer wall to line of maximum velocity	ft

Arabic Symbols	Description	Units
y^+_{1m}	Parameter: $y^+_{1m} = \left[\sqrt{\frac{\Delta A_1}{\Delta l_1 r_1}}\, r_1^{++}\, \frac{y_{1m}}{r_1}\right]$	-
y^+_{2m}	Parameter: $y^+_{2m} = \left[\sqrt{\frac{\Delta A_2}{\Delta l_2 r_1}}\, r_1^{++}\, \frac{y_{1m}}{r_1}\right]$	-

Greek Symbols	Description	Units
τ	Shear stress	lb_f/ft^2
ρ	Density	lb_m/ft^3
μ	Dynamic Viscosity	$lb_f/ft.sec.$

Letter Subscripts	Description	Units
1	Inner wall	-
2	Outer wall	-
0	Wall	-
m	Maximum	-

9. REFERENCES

1. Deissler, R. G.
   Taylor, M. F.
   "Analysis of Fully Developed Turbulent Heat Transfer and Flow in an Annulus with Various Eccentricities", N.A.C.A.-TN 3451, May 1955.

2. Heyda, J. F.
   "Heat Transfer in Turbulent Flow through Non-Concentric Annuli Having Unequal Heat Release from the Walls", A.P.E.X.-391, June 1957.

3. Ivey, C. M.
   "The Position of Maximum Velocity in Annular Flow", M.A.Sc. Thesis, University of Windsor, 1965.

4. Wilson, N. W.
   "A Theoretical Analysis of the Velocity Fields in Eccentric Annuli", M.Eng. Thesis, McMaster University, 1966.

5. van Driest, E. R.
   "The Turbulent Boundary Layer with Variable Prandth Number", Jahrb. 1954 der Wiss. Ges. F. Luftfahrt, 1966.

6. Lee, Y.
   Barrow, H.
   "Turbulent Flow and Heat Transfer in Concentric and Eccentric Annuli", Proc. Instn. Mech. Engrs., Vol. 178, Pt 31(iv), 1963-64.

7. Goel, R. K.
   "An Experimental Determination of Settling Length for Turbulent Flow of Air in Annular Ducts", M.A.Sc. Thesis, Windsor University, 1965.

8. Judd, R. L.
   "Turbulent Forced Convection Heat Transfer in Annular Passages", M. Eng. Thesis, McMaster University, 1963.

9. Richmond, R. L.
   "Experimental Investigation of Thick, Axially Symmetric Boundary Layers on Cylinders at Subsonic and Hypersonic Speeds", California Institute of Technology, Memorandum No 39, 1957.

10. ILLUSTRATIONS

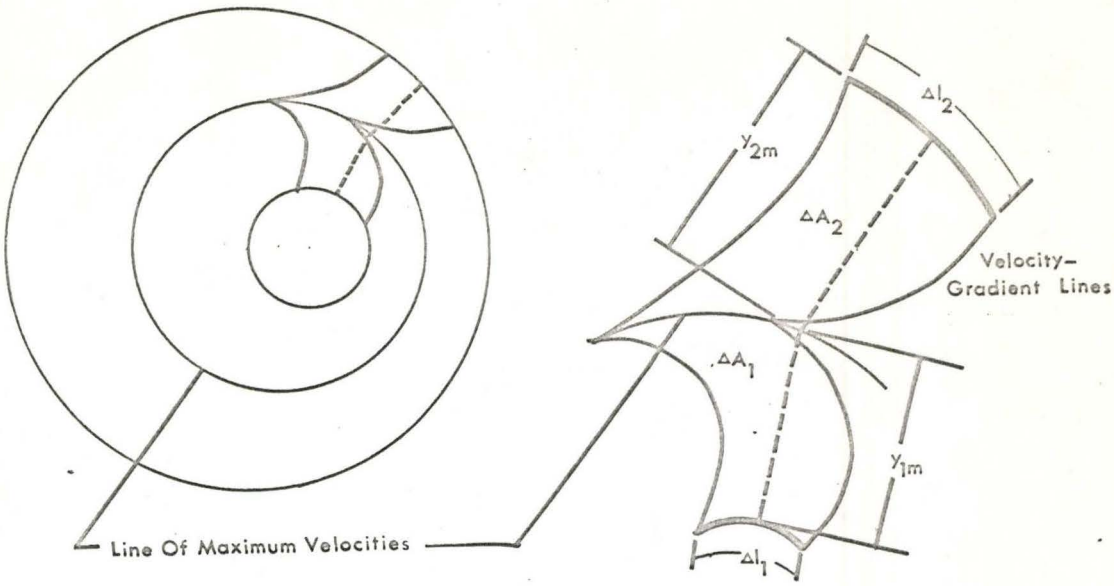

Annulus Analysis, First Iteration (Taken from Deissler and Taylor (1))

Figure 1

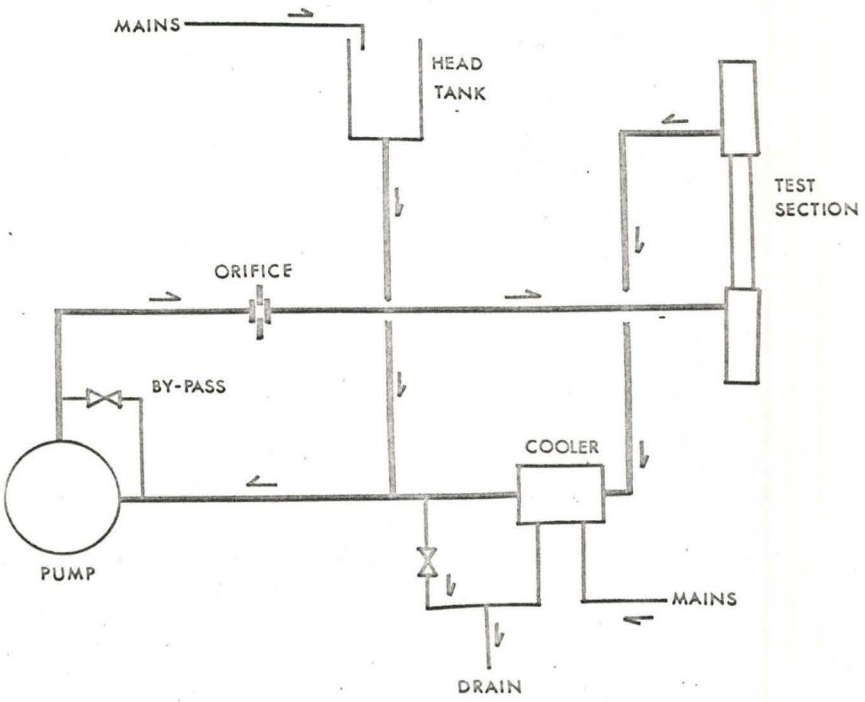

Schematic Arrangement of Test Facility Components

Figure 2

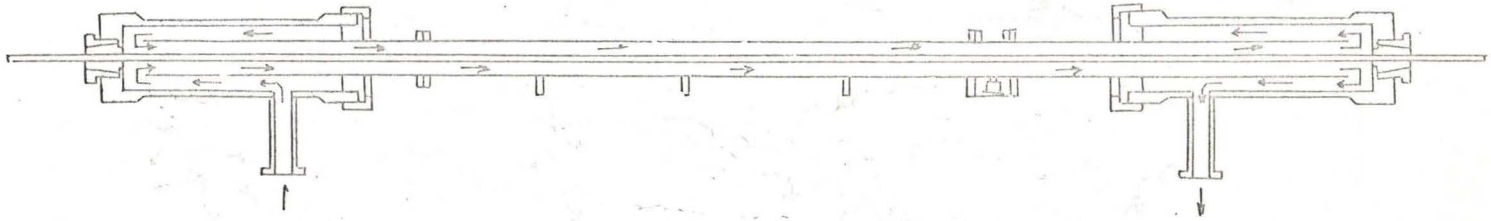

Flow Path in the Test Section

Figure 3

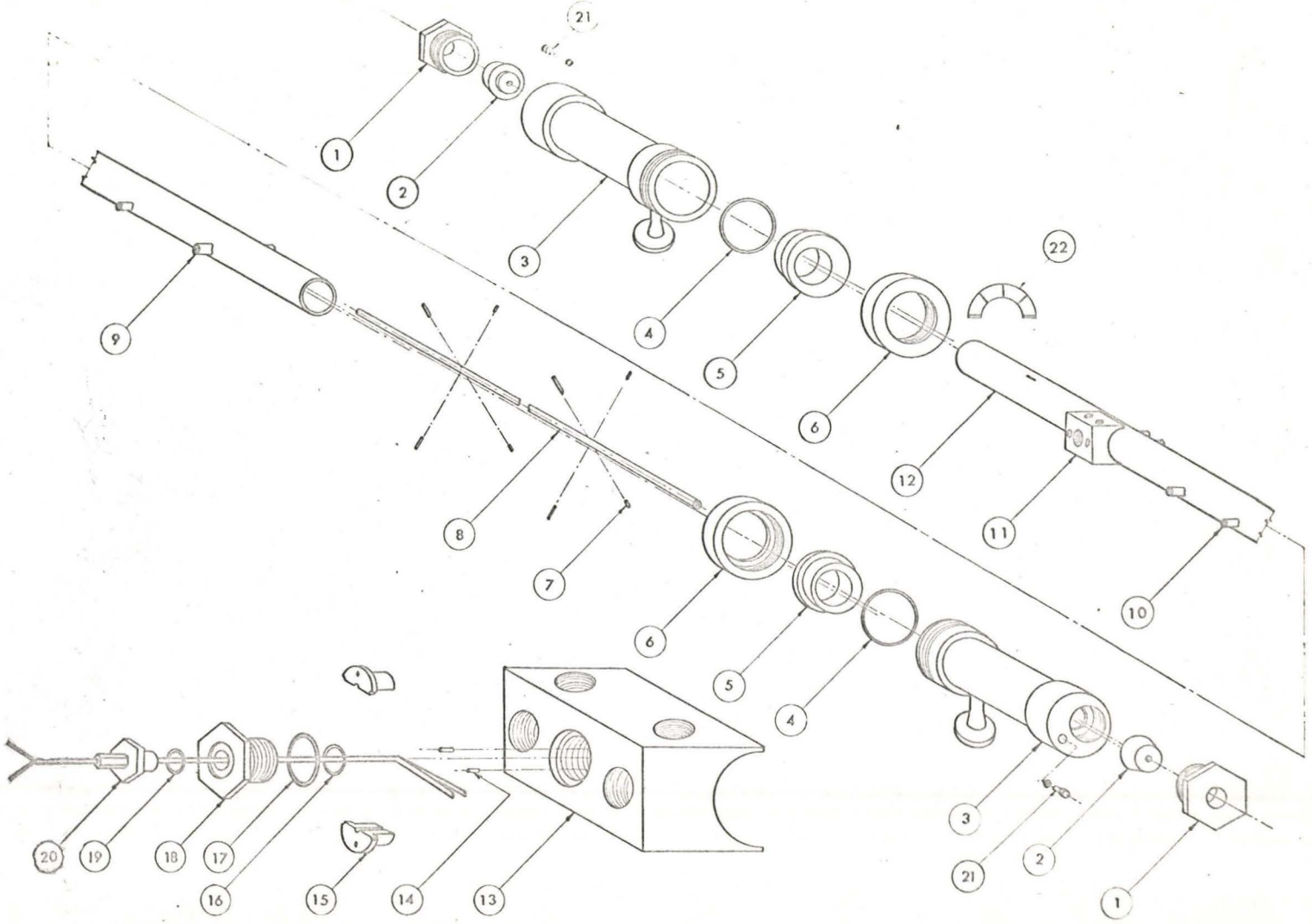

Exploded View of the Test Section

Figure 4

PARTS LIST EXPLODED VIEW

PART No.	DESCRIPTION
1.	Brass Nut
2.	Teflon Bushing (tapered) to Clamp and Seal Inner Rod
3.	Stainless Steel Housing
4.	"o" Ring
5.	Eccentric Hub
6.	Acrylic Nut Used to Hold Eccentric Hub in Place
7.	Acrylic Locating Legs
8.	Inner Rod (brass)
9.	Static Pressure Measuring Station
10.	Dial Gauge Access Fitting
11.	Measurement Station
12.	Outer Tube
13.	Acrylic Plastic Block
14.	Locating Dowel
15.	Split Brass Bushing
16.	Packing "o" Ring
17.	Sealing "o" Ring
18.	Brass Nut, Drilled and Spotfaced
19.	"o" Ring
20.	"Swagelok" Fitting, Drilled to .072 inch I.D.
21.	Drain Plug and "o" Ring
22.	Protractor

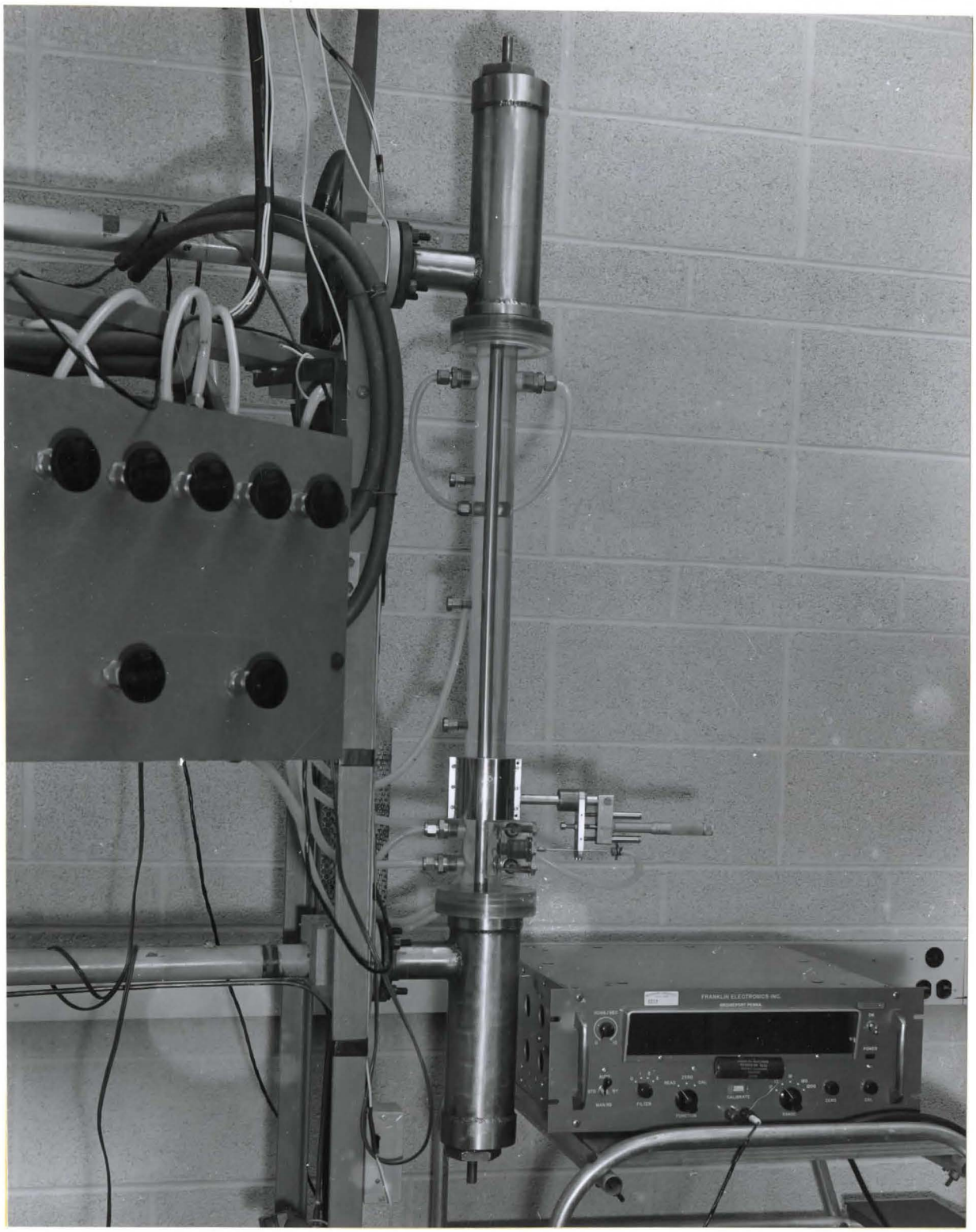

Test Facility
(Probe in upstream position)

Figure 5

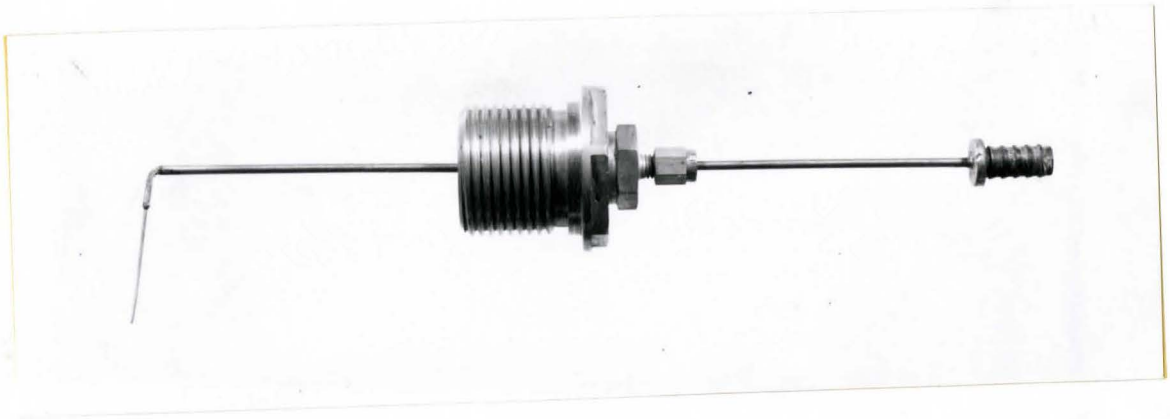

Obtuse Stagnation Probe

Figure 6

Acute Stagnation Probe

Figure 7

Double-tipped Stagnation Probe

Figure 8

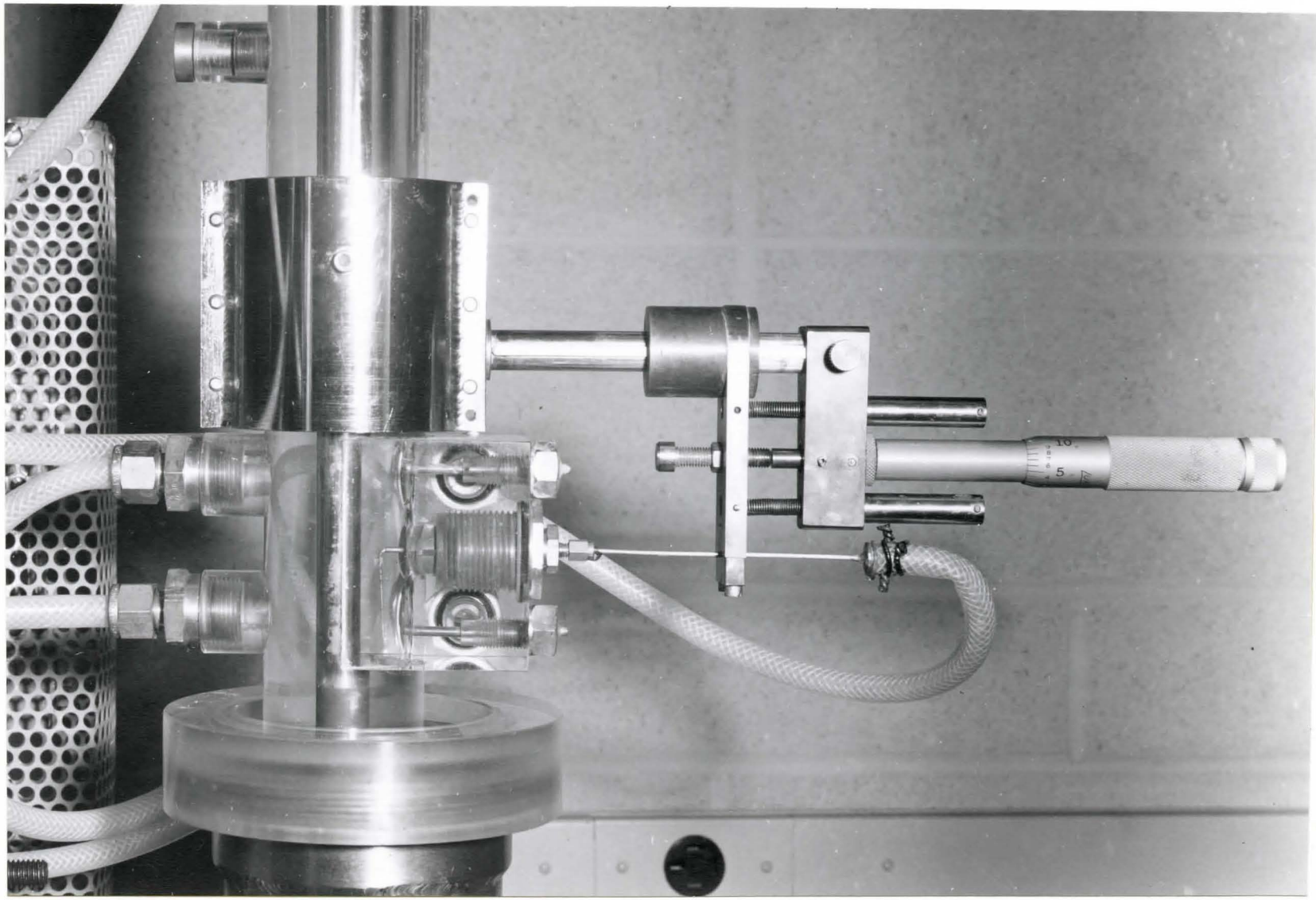

Traversing Mechanism and Measuring Block

Figure 9

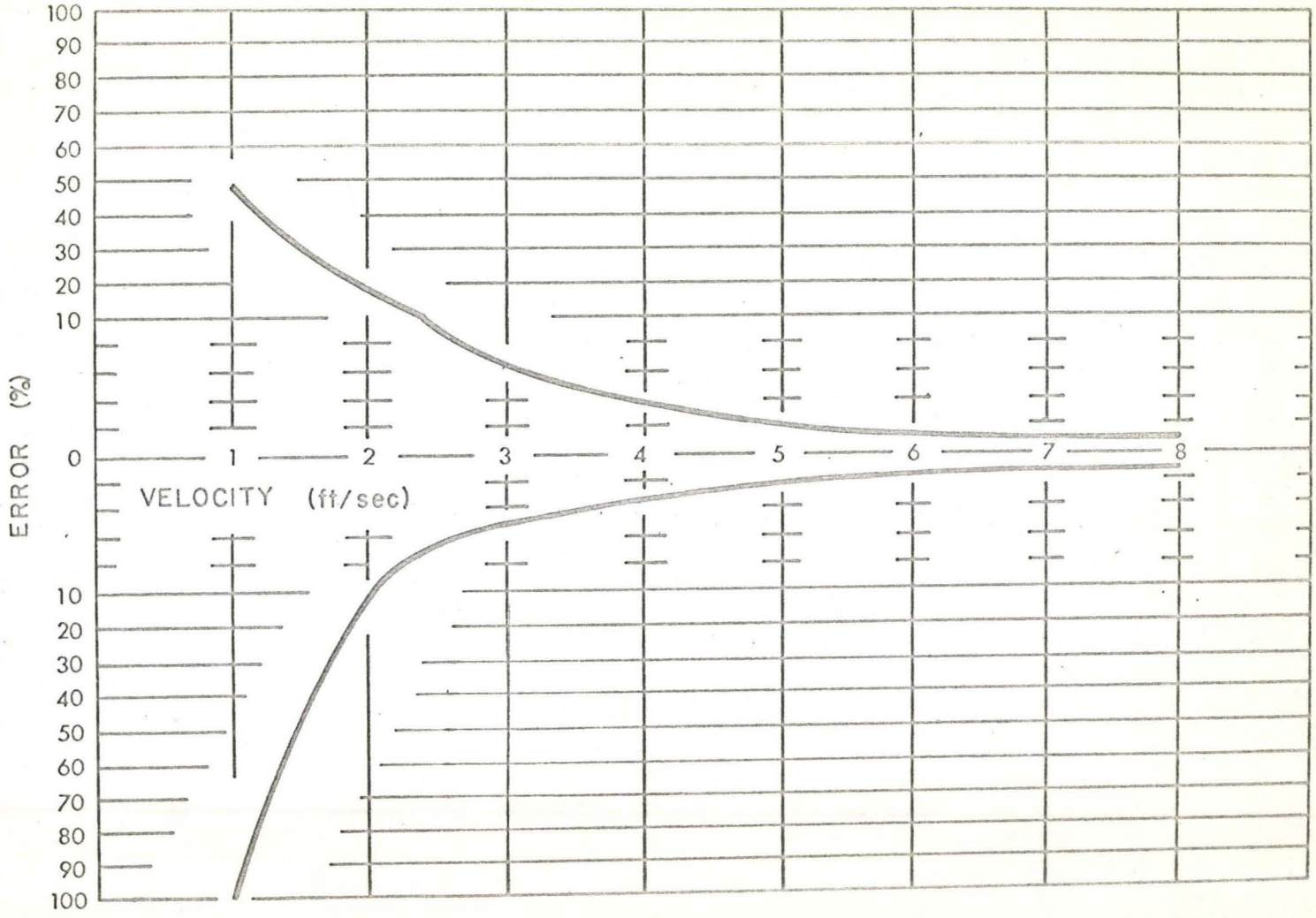

Error versus Velocity

Figure 10

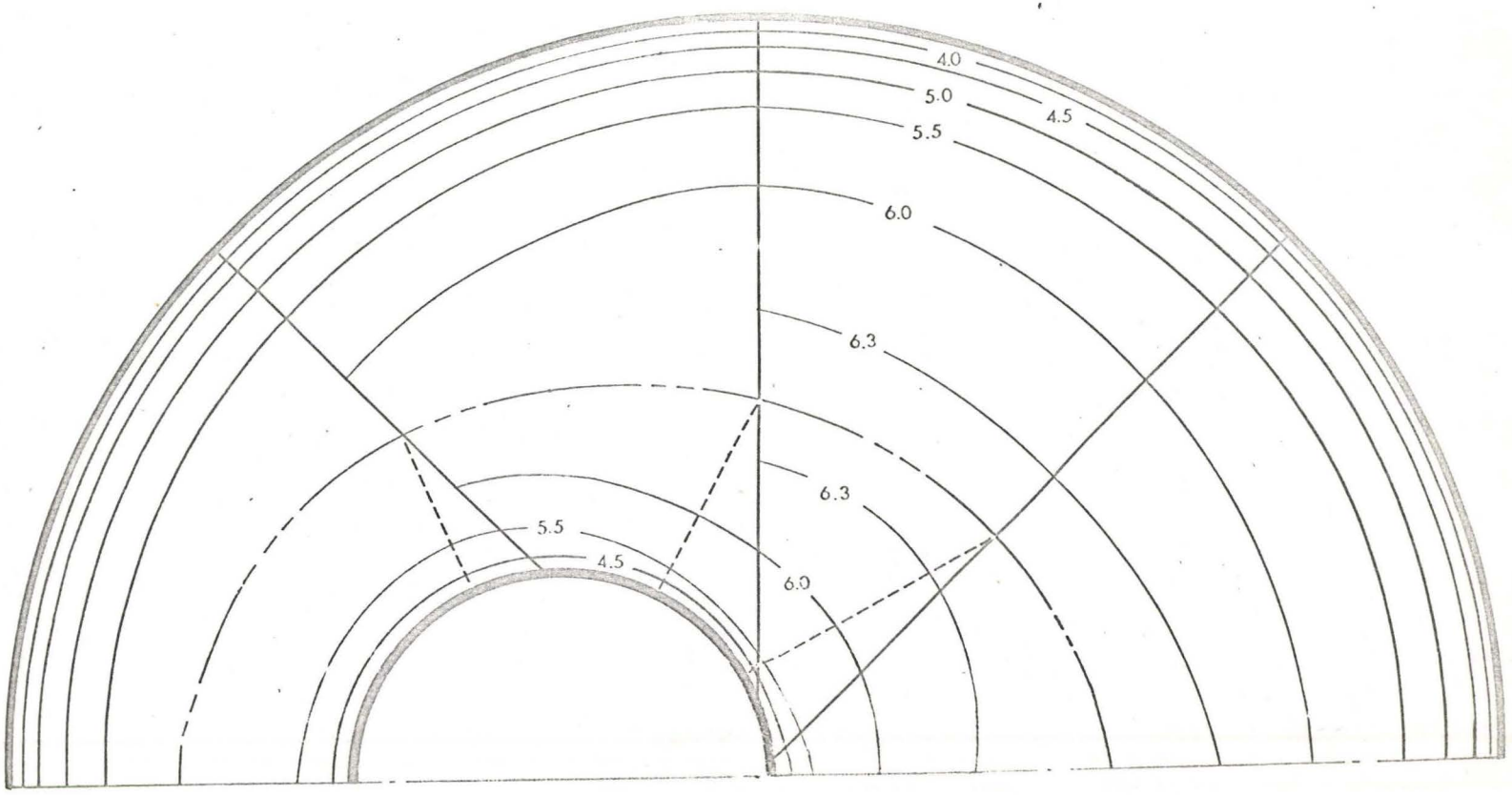

Velocity Field in a 36.5% Eccentric Annulus at a Reynolds Number of 80,000

Figure 11

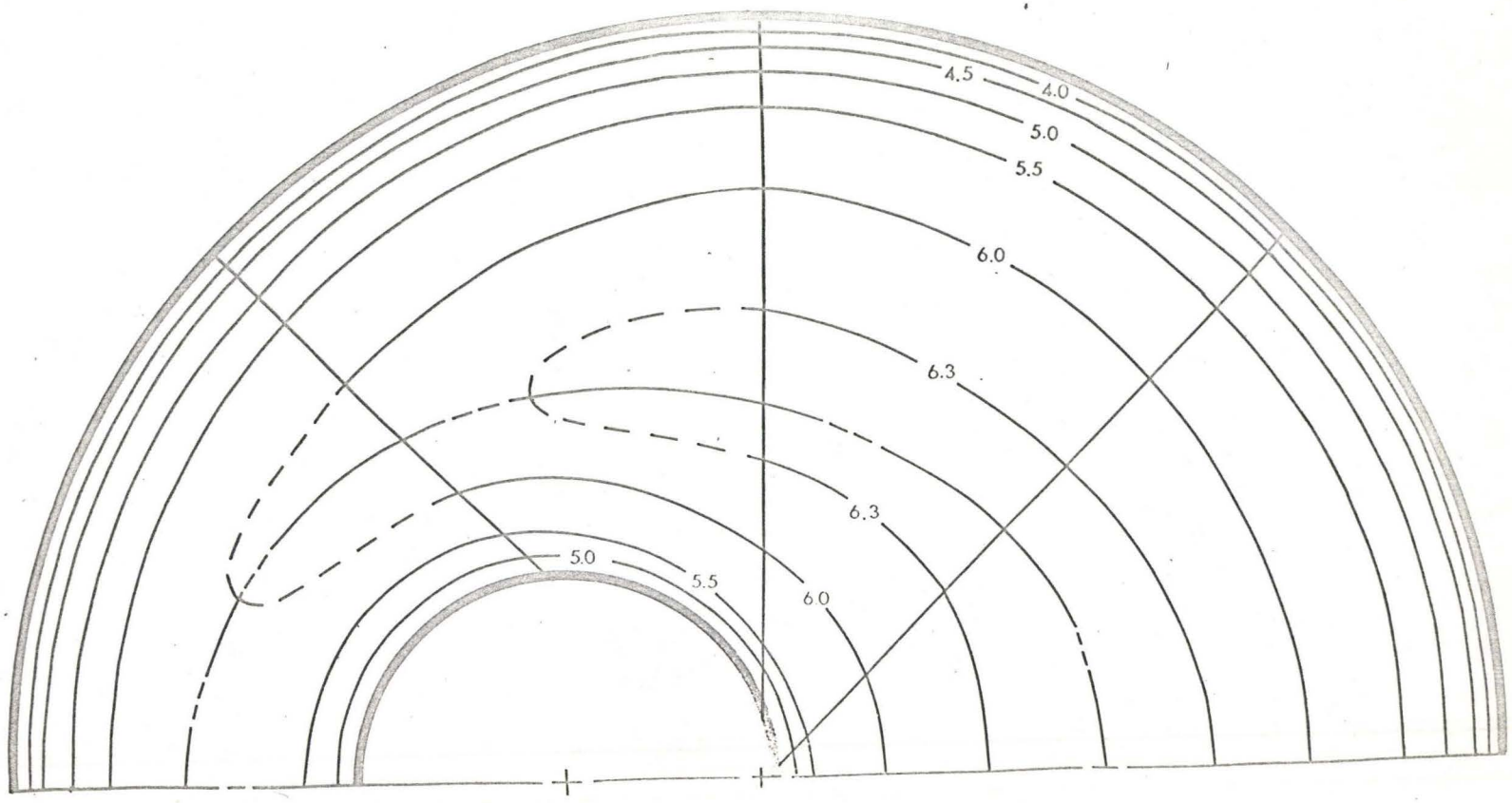

Revised Velocity Field in a 36.5% Eccentric Annulus at a Reynolds Number of 80,000

Figure 12

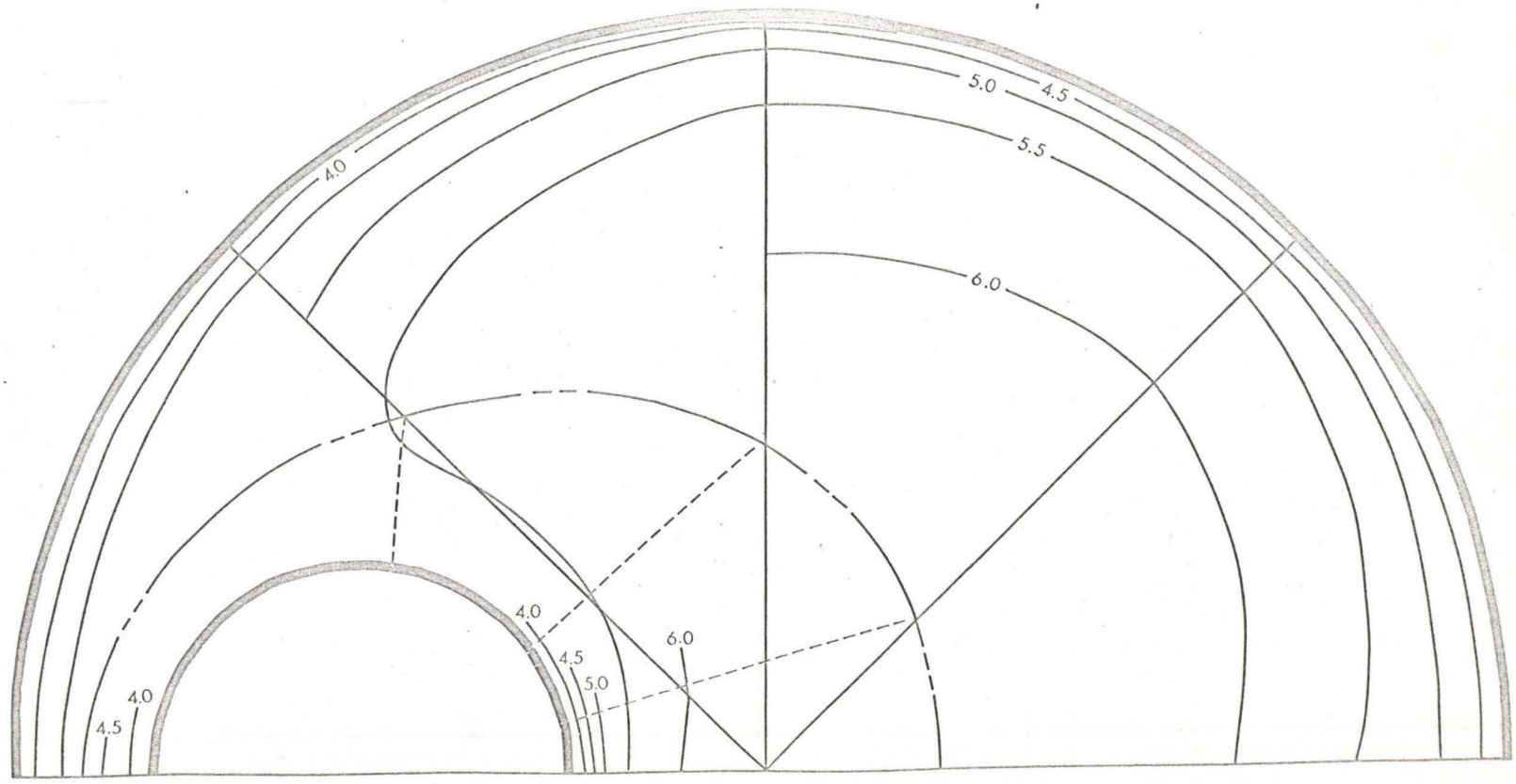

Velocity Field in a 76.0% Eccentric Annulus at a Reynolds Number of 80,000

Figure 13

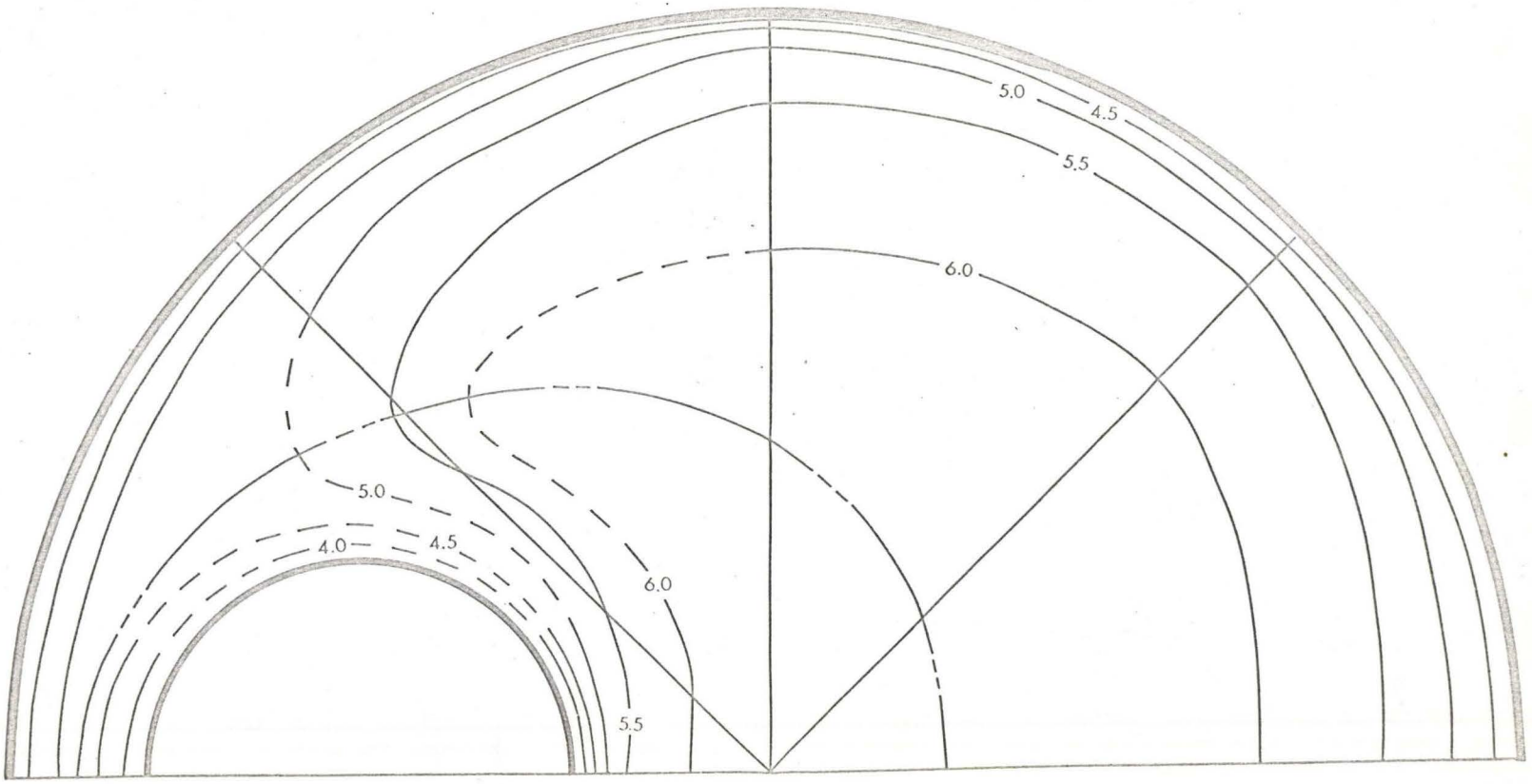

Revised Velocity Field in a 76.0% Eccentric Annulus at a Reynolds Number of 80,000

Figure 14

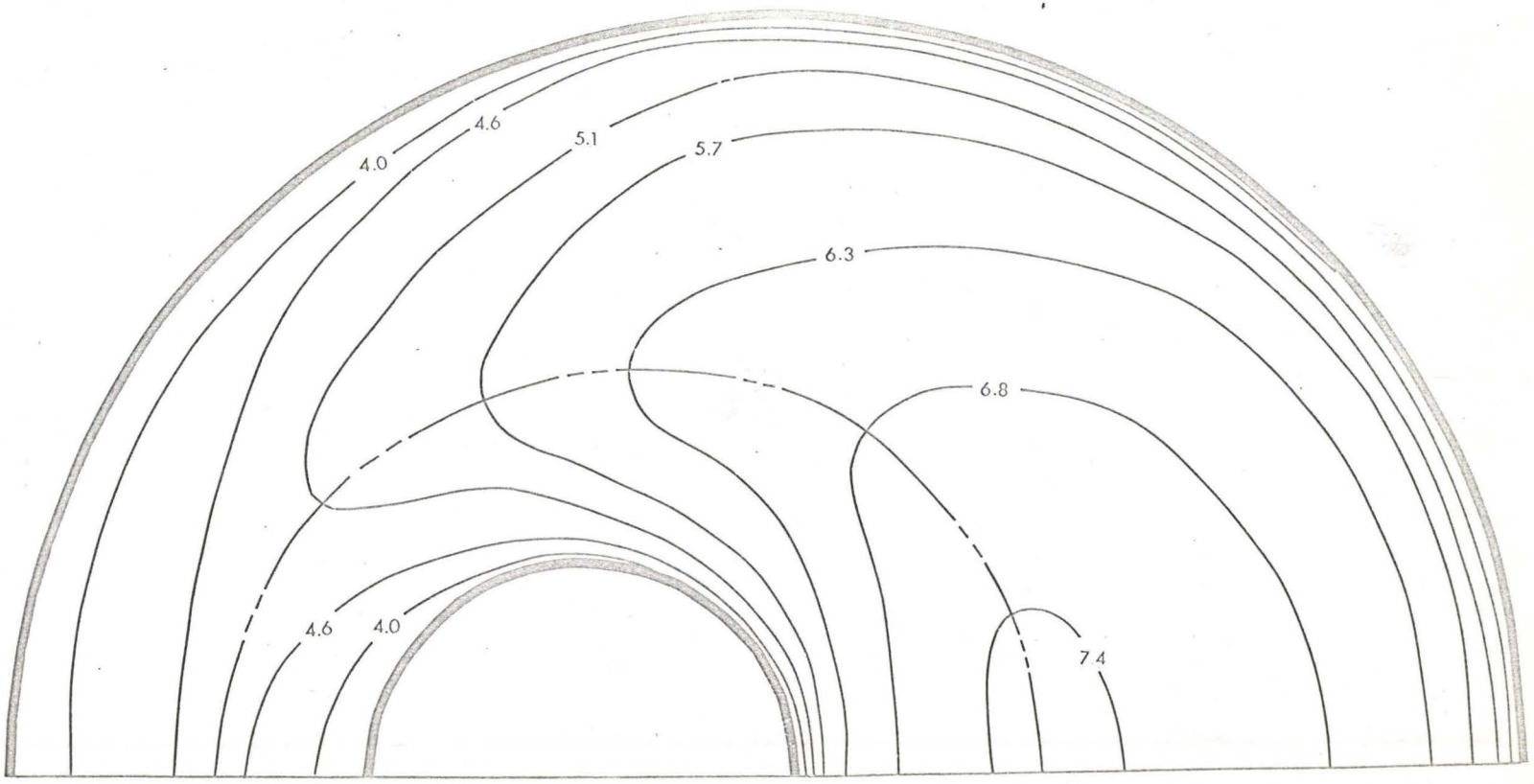

Theoretical Velocity Field in a 36.5% Eccentric Annulus at a Reynolds Number of 80,175

Figure 15

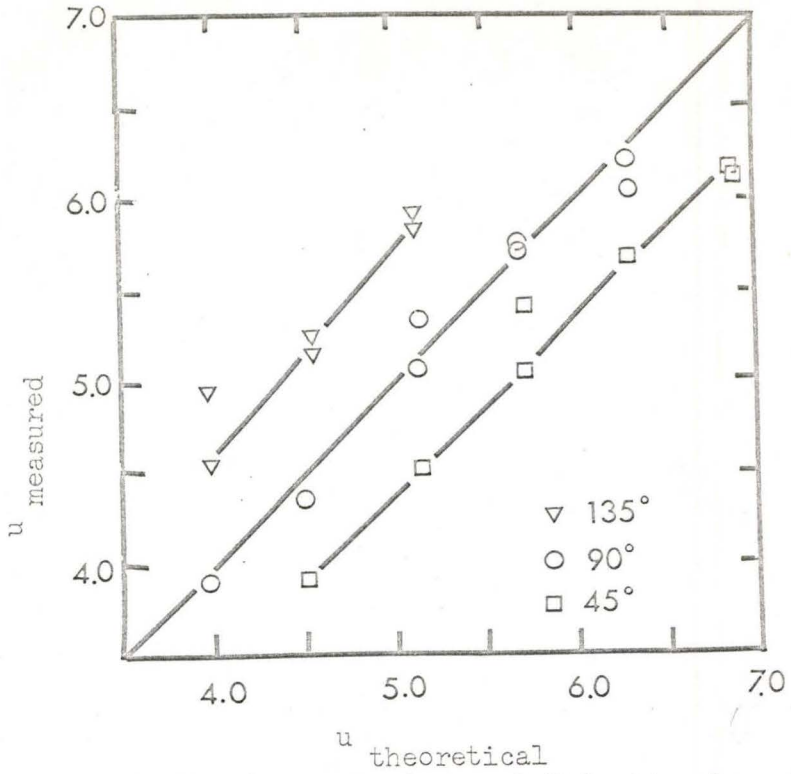

Figure 16 - Measured Velocity versus Theoretical Velocity along Three Measuring Radii

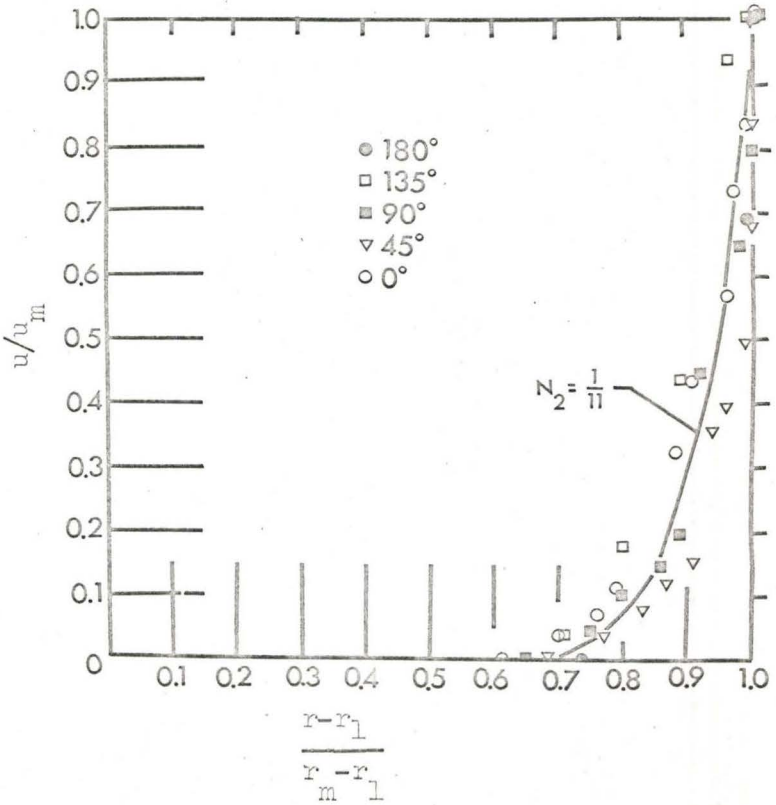

Figure 17 - Inner Wall Dimensionless Velocity Profile (36.5% Eccentricity, 80,000 Reynolds Number)

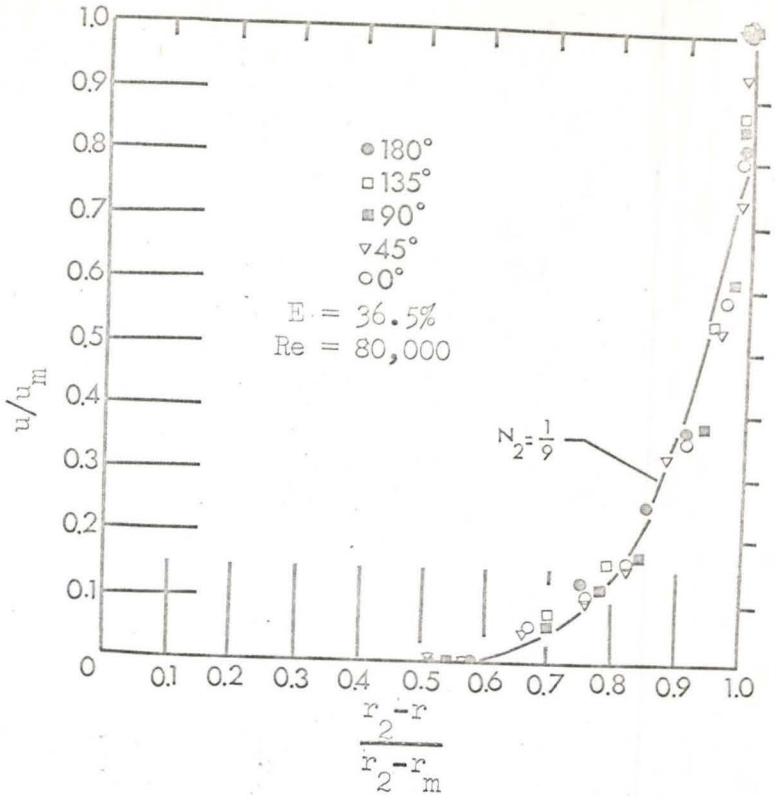

Figure 18 - Outer Wall Dimensionless Velocity Profile

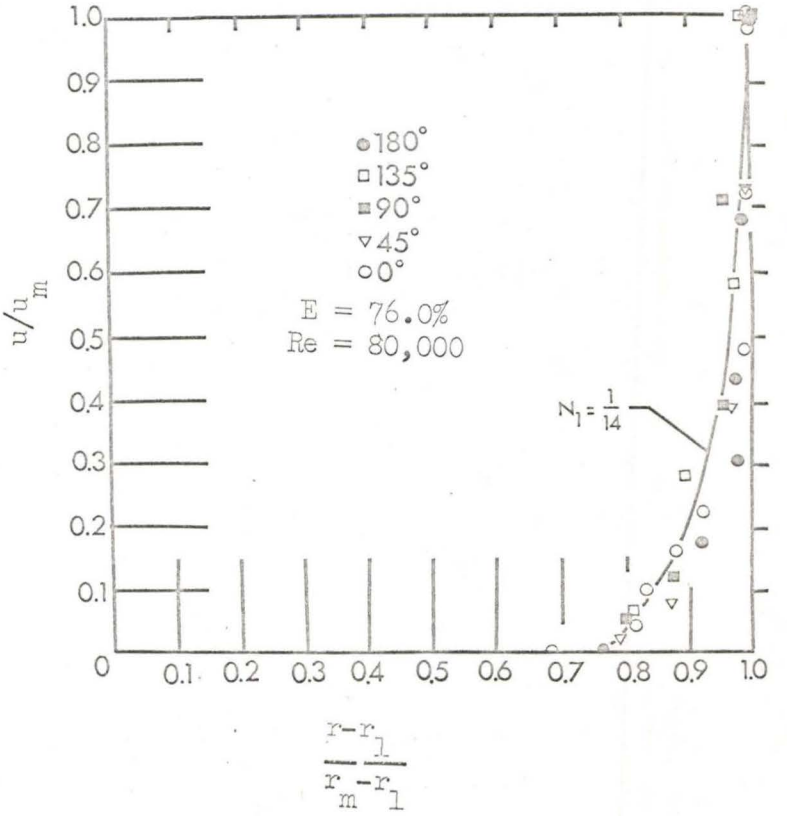

Figure 19 - Inner Wall Dimensionless Velocity Profile

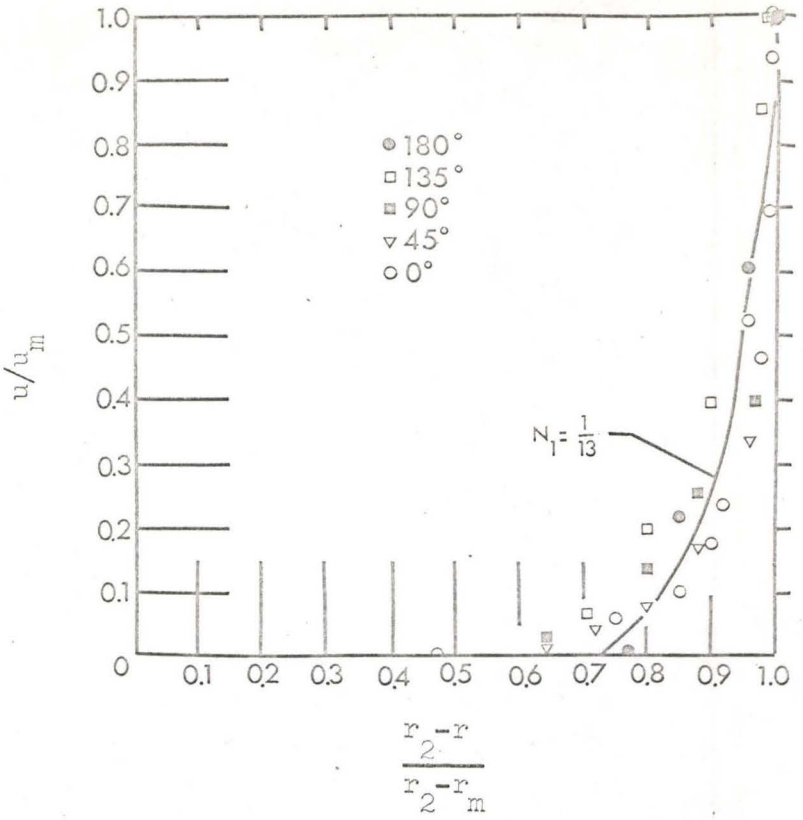

Outer Wall Dimensionless Velocity Profile
(76.0% Eccentricity, 80,000 Reynolds Number)

Figure 20

APPENDIX

1. Velocity Correlation

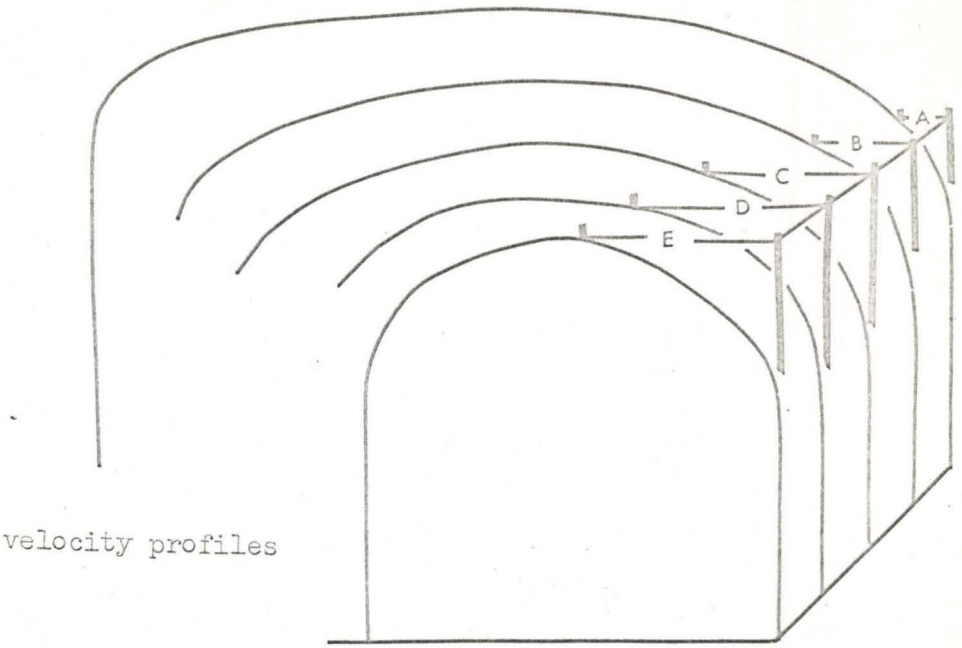

velocity profiles

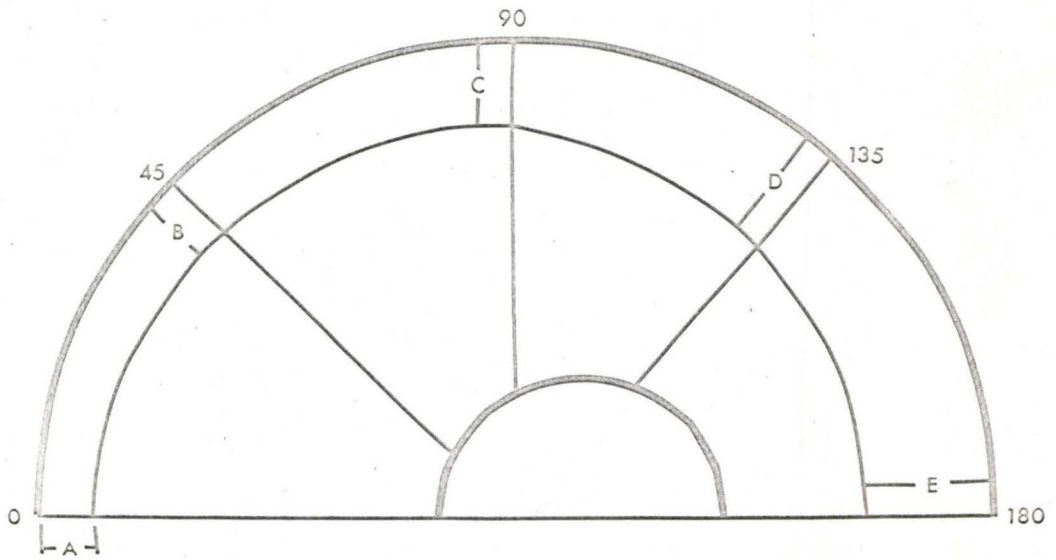

Annulus Cross-section

Figure 1

2. Velocity Profiles

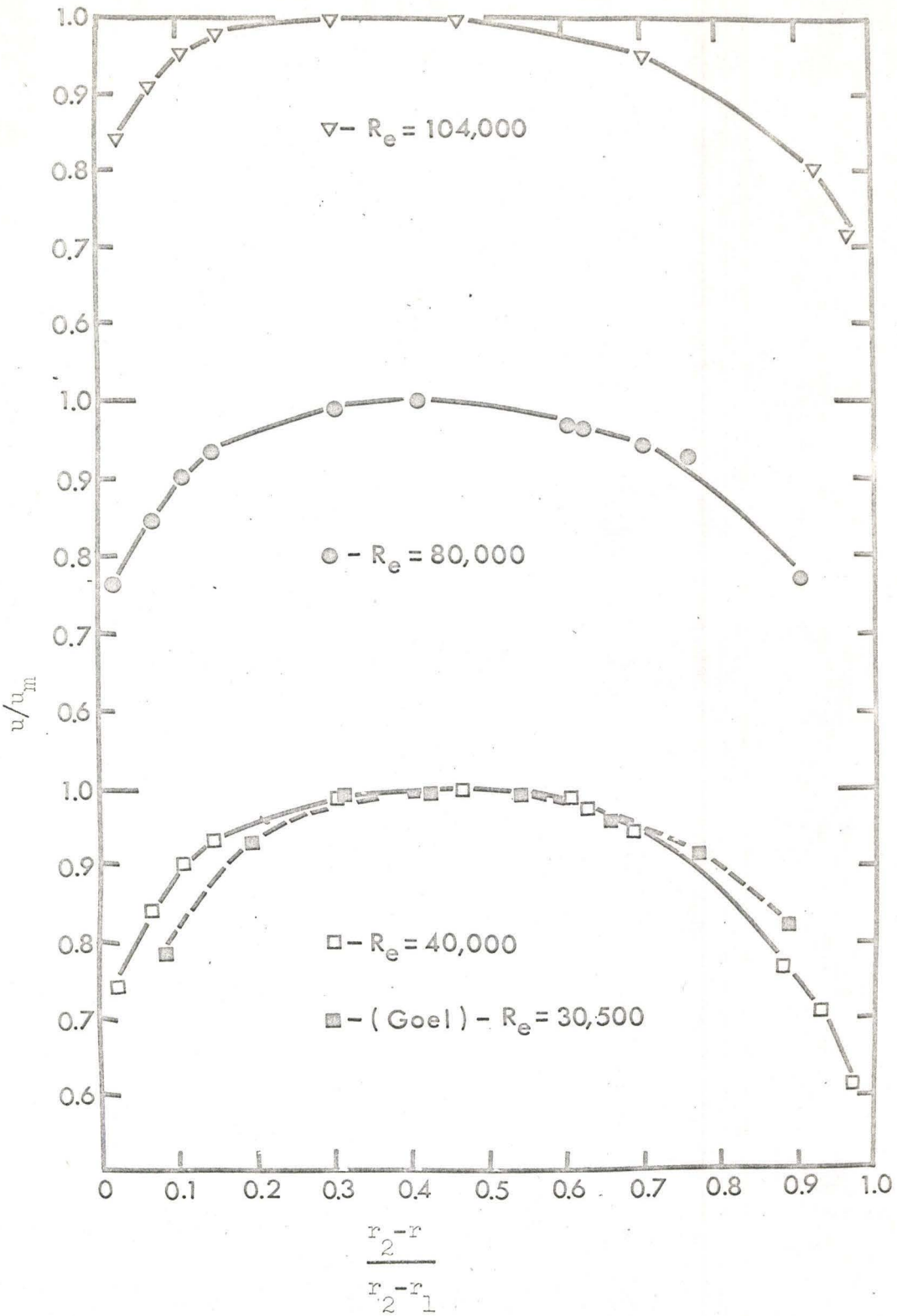

Figure ii

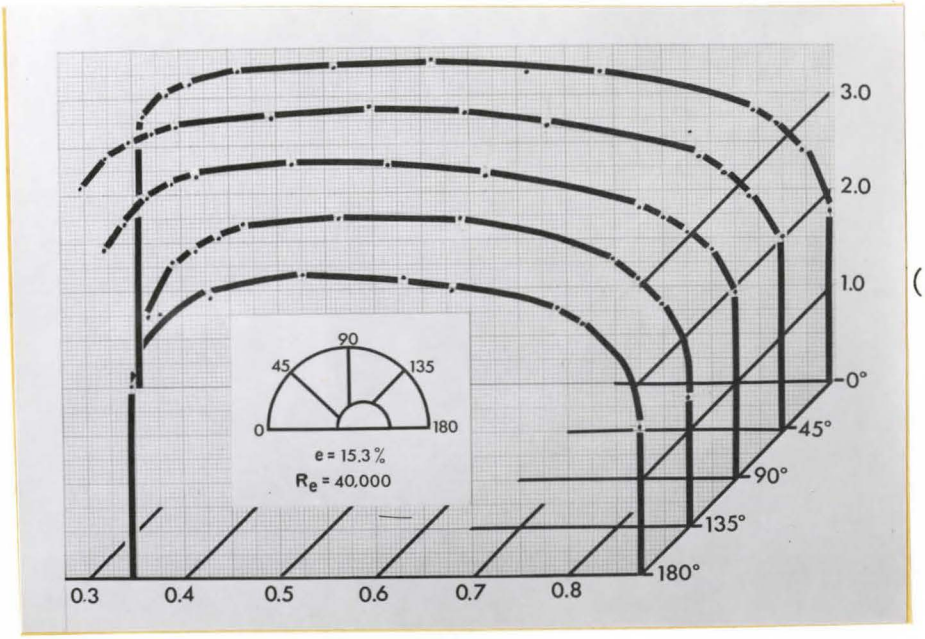

Figure iii

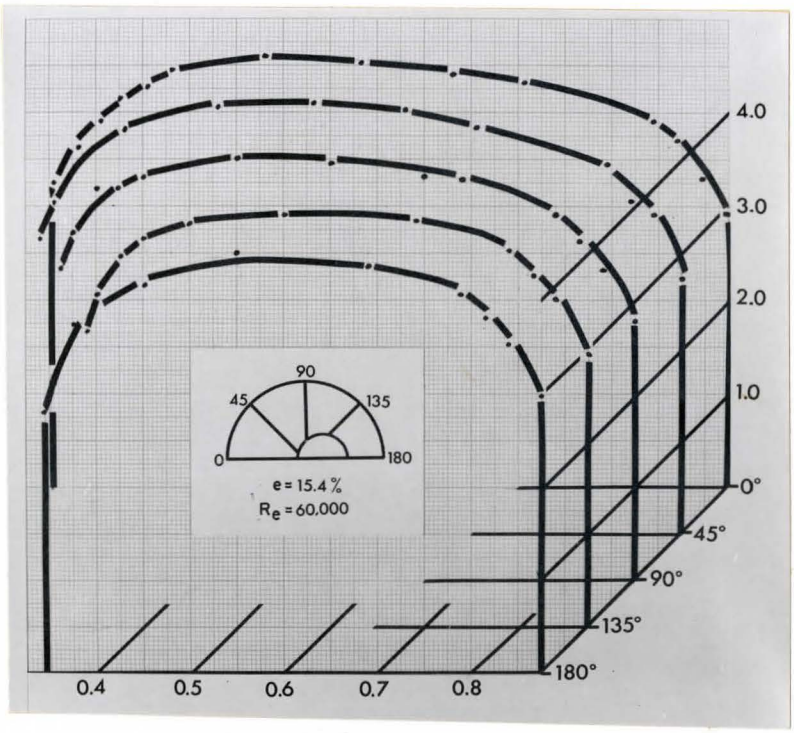

Figure iv

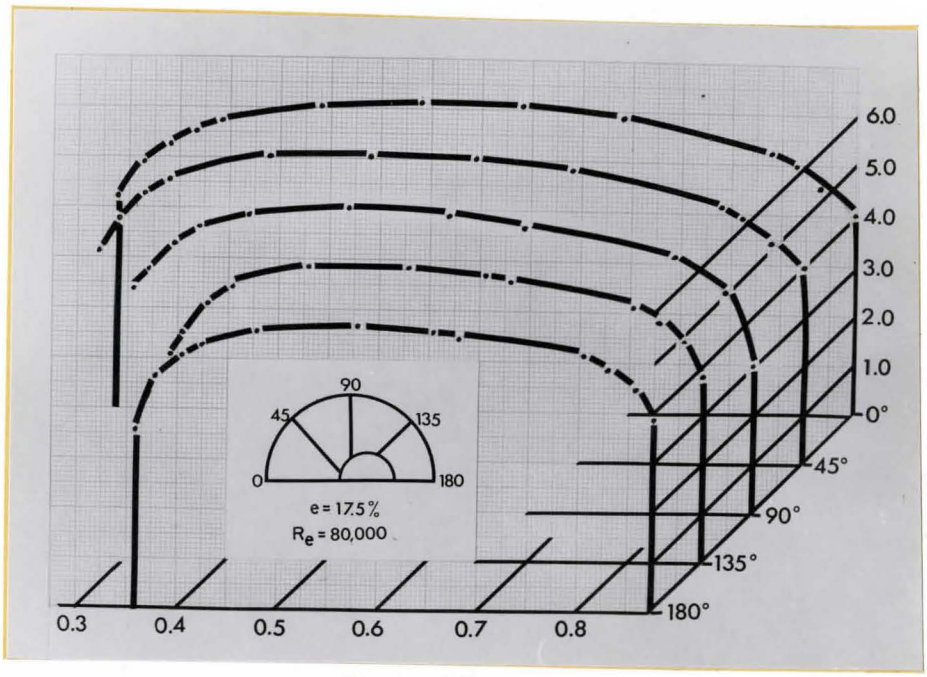

Figure v

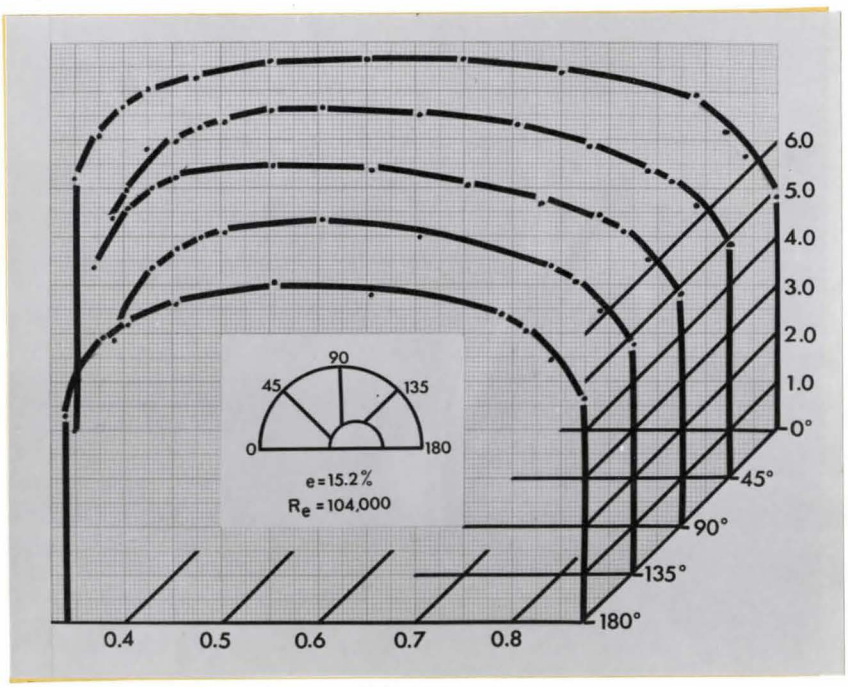

Figure vi

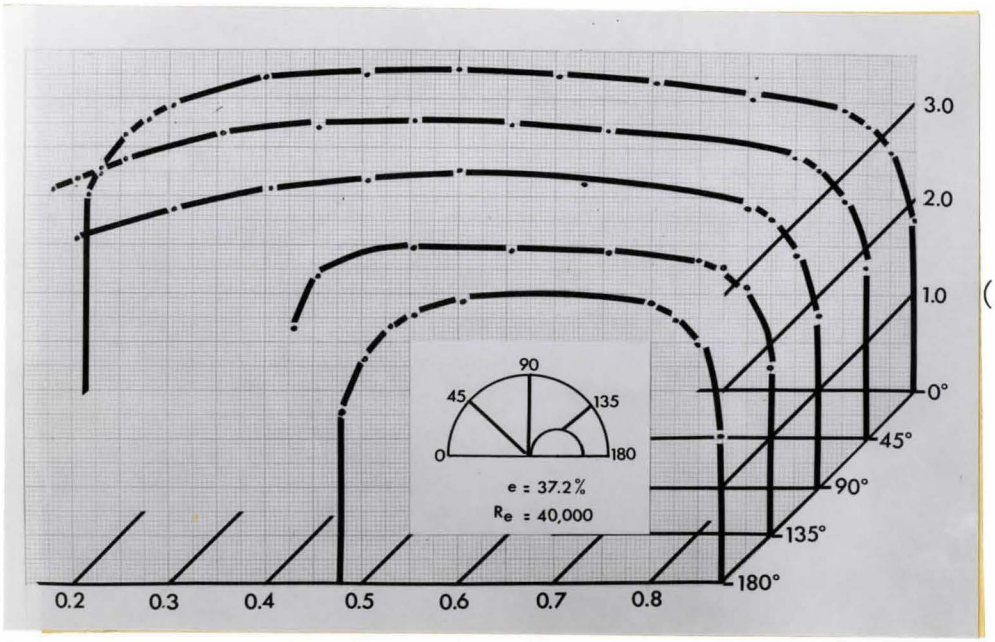

Figure vii

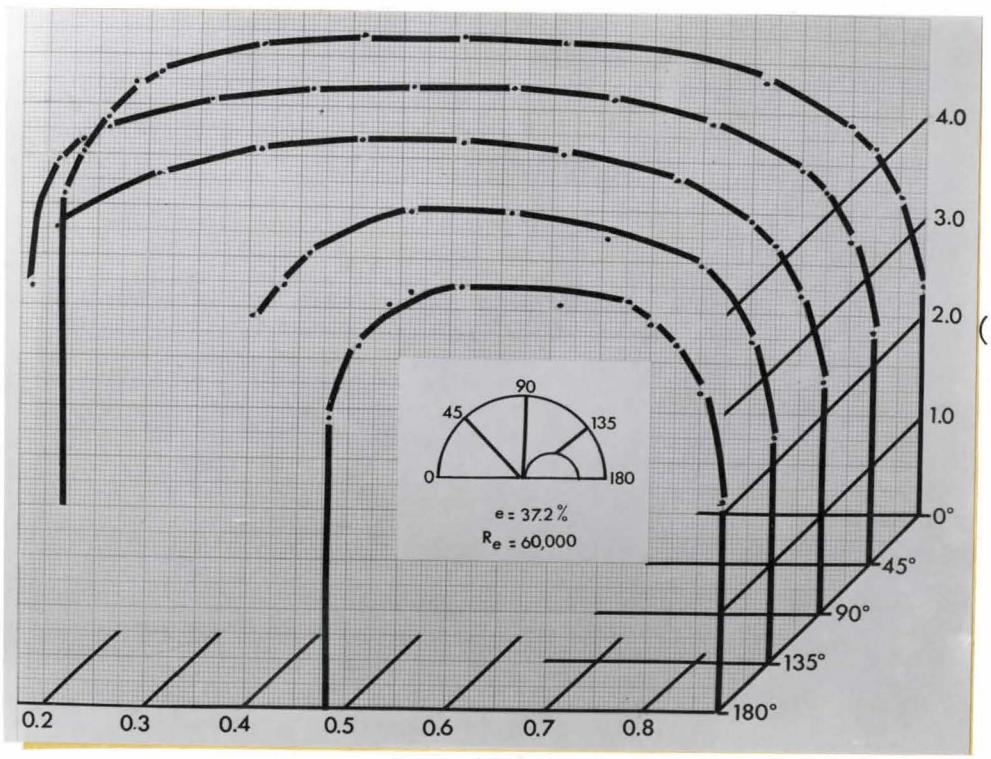

Figure viii

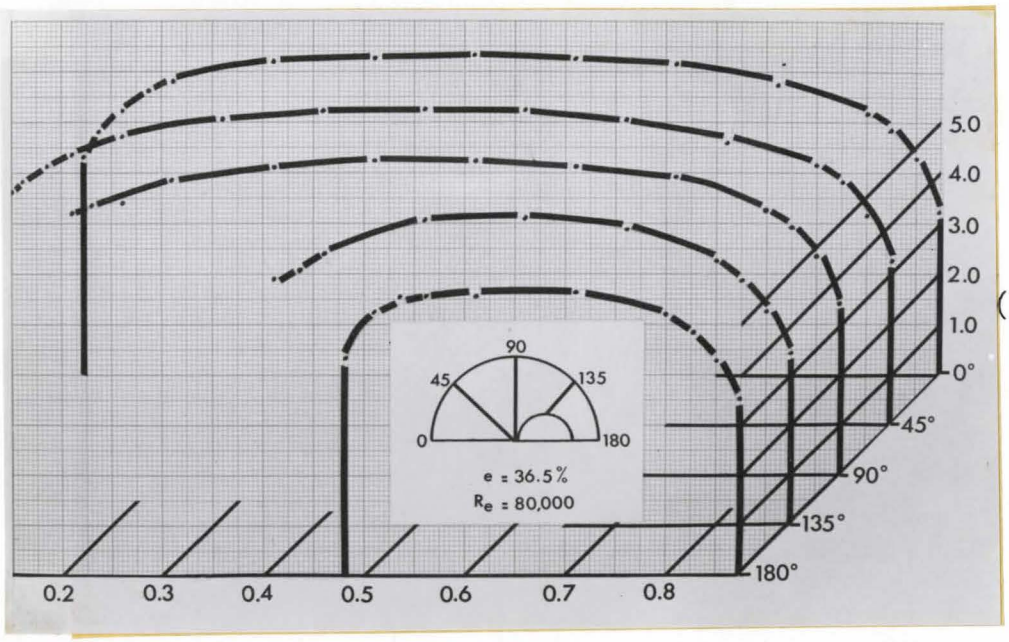

Figure ix

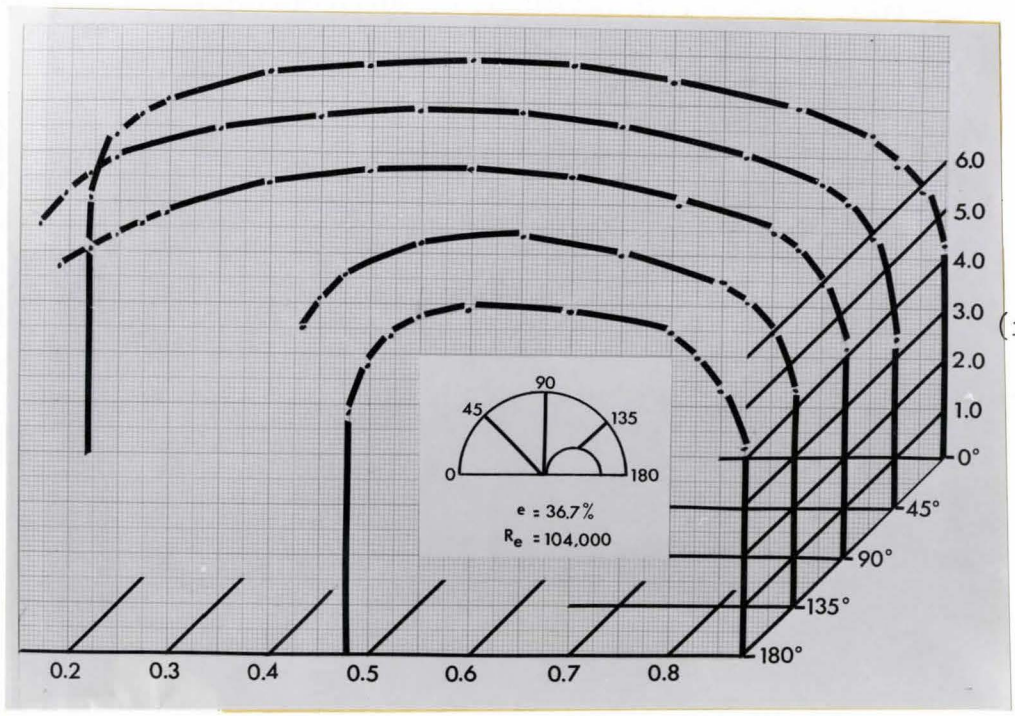

Figure x

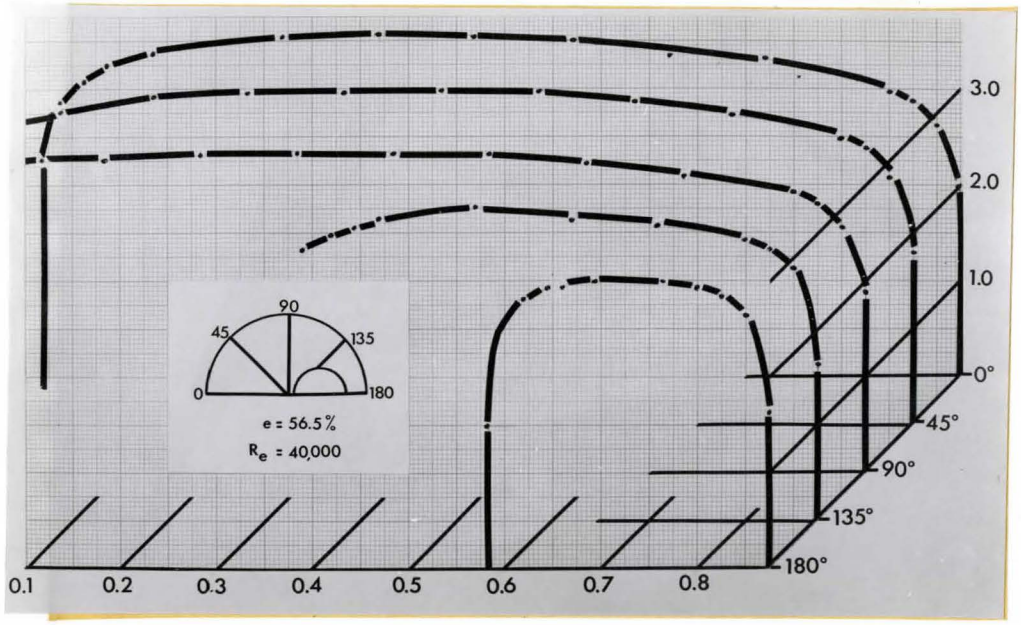

Figure xi

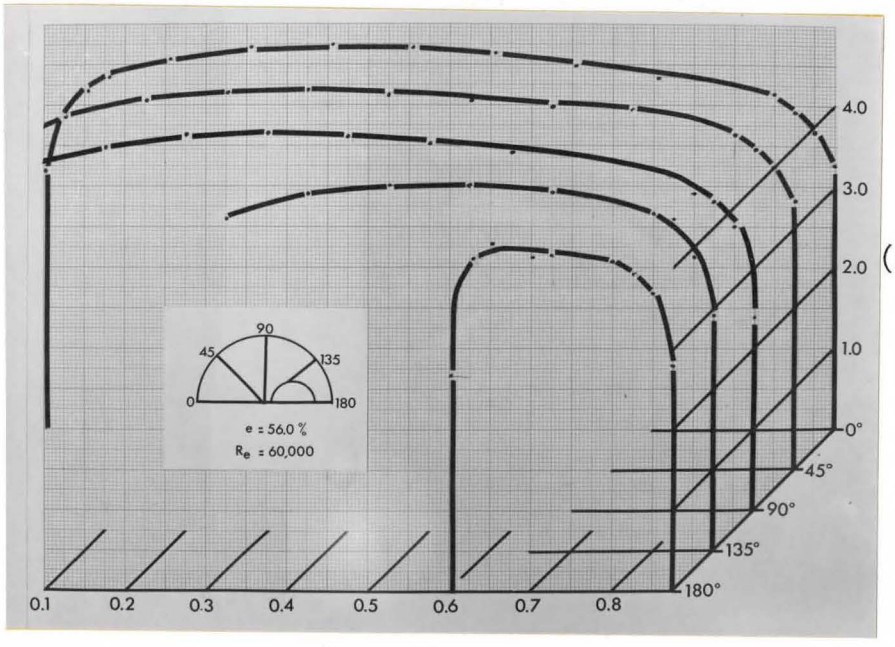

Figure xii

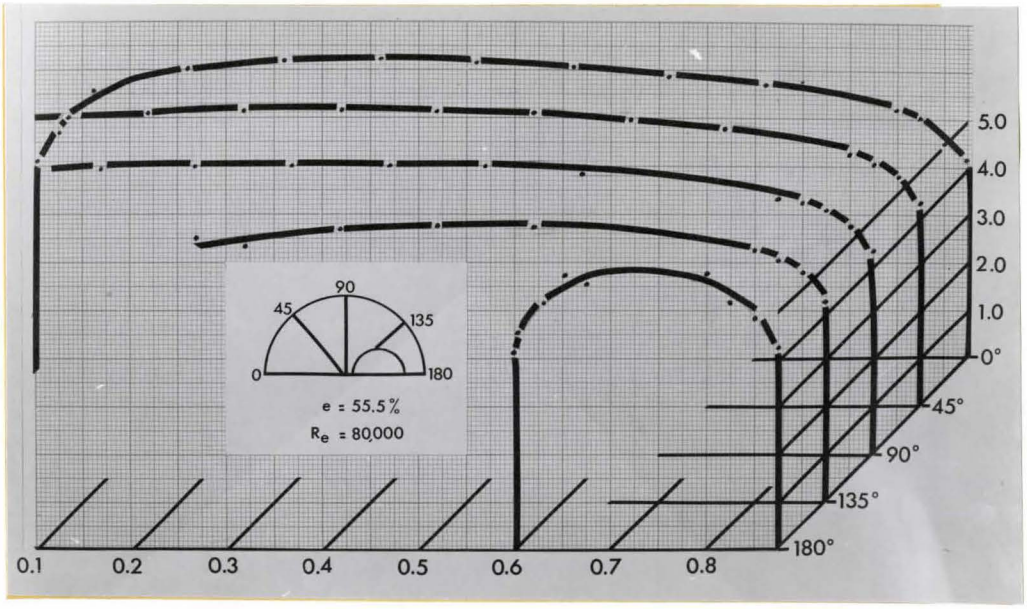

Figure xiii

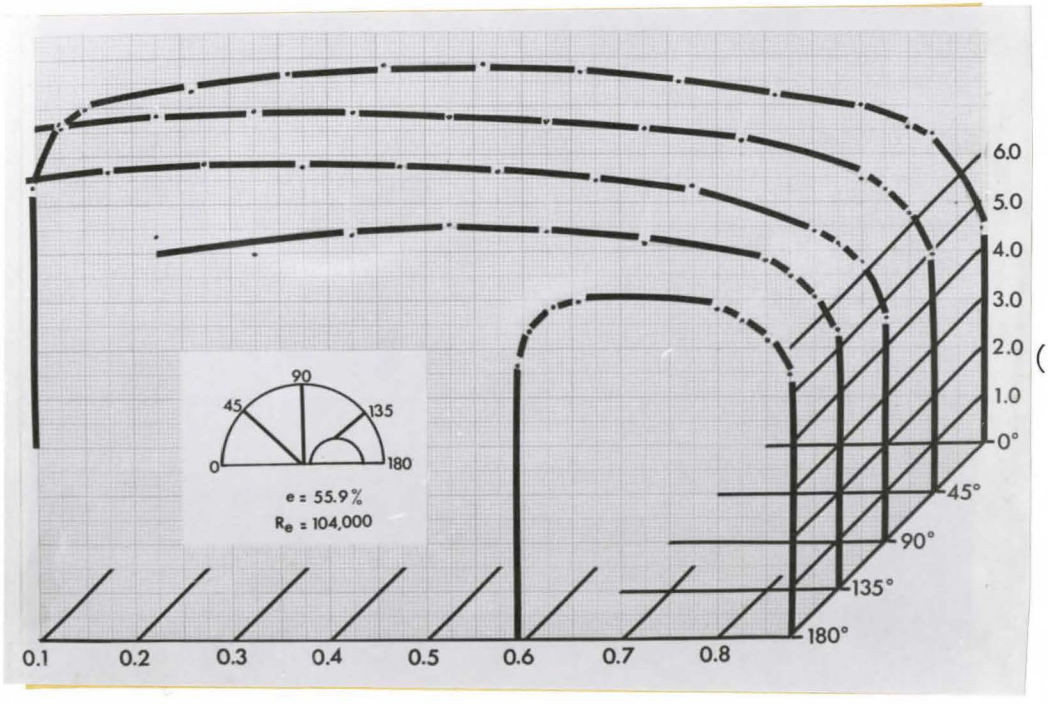

Figure xiv

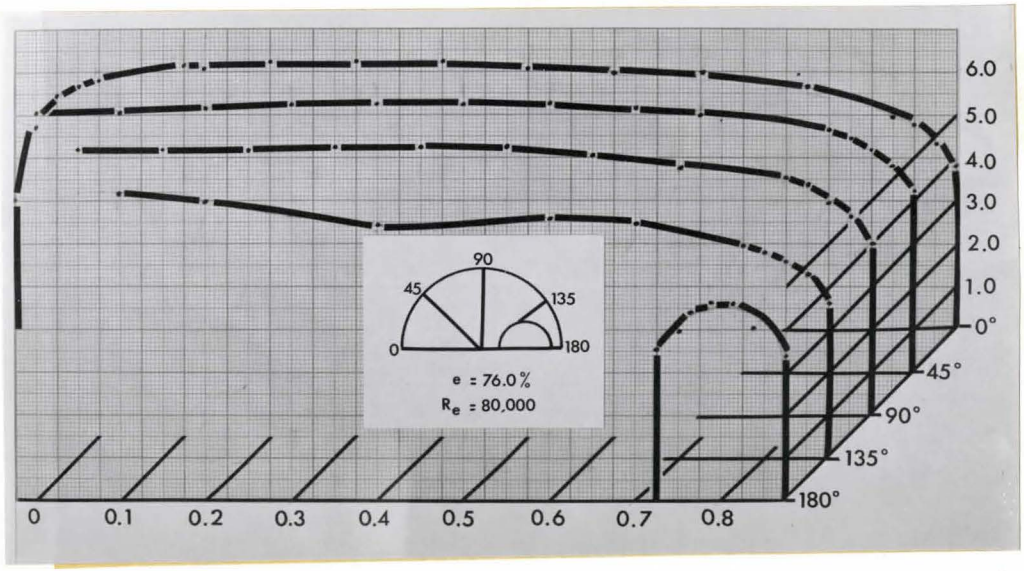

Figure xv

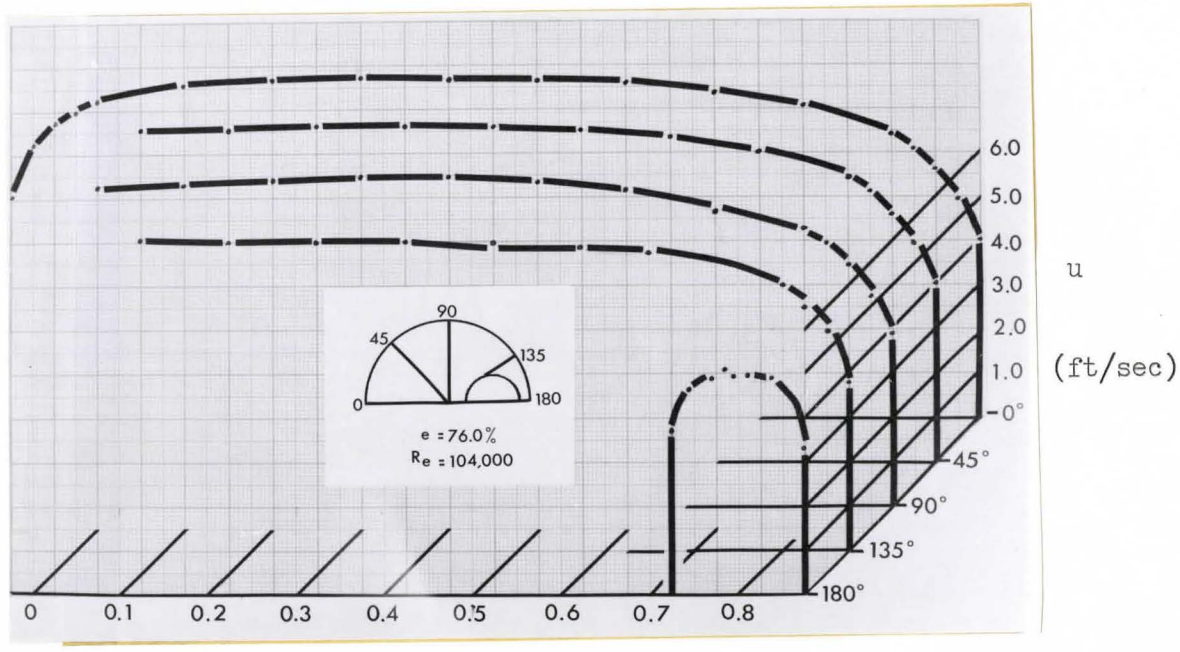

Figure xvi